13.8 Geochemistry of Magmatic Ore Deposits

JE Mungall, University of Toronto, Toronto, ON, Canada

13.8.1 Introduction

Magmatic ore deposits are masses of igneous rock enriched in useful chemical elements to such an extent that it is feasible to mine them at a profit. To be considered an ore, an accumulation of an element must combine high grade with large tonnage and must be accessible to mining operations. Since the definition of ore is more cultural than geochemical, this chapter avoids lists of grades and tonnages of individual orebodies and focuses instead on the underlying geochemical processes through which high concentrations of the elements can arise. There is an overlap between magmatic and hydrothermal processes because fluids coexist with magmas over wide ranges of temperature and pressure (see **Chapter 13.1**). The low density and viscosity of fluids permit their rapid physical separation from magmatic systems in many examples and allow a clean conceptual separation between most classes of hydrothermal and magmatic ore deposits (e.g., hydrothermal porphyry deposits and magmatic chromitite deposits). However, there are also some deposit types that may owe their origins to complex fluid–melt interactions over a range of temperatures.

This chapter provides brief descriptions of the major types of magmatic ore deposits, focusing on their compositions and the geochemical and petrogenetic processes by which they might form. For detailed descriptions of the ore deposits themselves, the reader is referred to any of the many reviews available. In most cases, references have been chosen to highlight important recent studies of the particular geochemical issues at hand, rather than to provide a comprehensive list of references spanning several decades. It is unavoidable, therefore, that some of the original presentations of key concepts are not cited here, and apologies are offered to the authors of those studies.

The generation of any ore deposit depends on the presence of a source for the element, a transporting medium, and a trap in which it may be concentrated. In general, the source rock contains the element of interest at concentrations very far below ore grades. Although it may be useful to consider some lithotectonic environments as being intrinsically fertile ground from which to generate magmas with high initial concentrations of economically interesting elements, most ore-forming magmas originate by melting of mantle peridotite (see **Chapter 3.10**), and it is the melting process itself that determines whether the resulting magma will have the potential to form an ore deposit, because of the homogenizing effects of melting in large volumes of source rock. Ore deposits form when the magma is transported to a new site and undergoes phase separation and mechanical sorting into small volumes of a phase rich in the elements of interest and large volumes of barren material (**Figure 1**). The collector phase may be a mineral, an immiscible melt such as sulfide liquid or carbonatite melt, or it may even be the silicate melt itself after an extended process of removal of barren mineral phases. In the early years of the twentieth century, the concept of liquid immiscibility as a major petrogenetic process was definitively laid to rest by the success of Bowen's crystallization–differentiation hypothesis in explaining the diversity of common igneous rock

types. However, the separation of an immiscible melt or fluid phase, or the failure to do so when most magmas would, is the key to the formation of most of the magmatic ore deposit types discussed here.

It is impossible to avoid some partisan choices in presenting the many competing hypotheses for the generation of magmatic ore deposits, but an attempt has been made to give a balanced view throughout.

13.8.2 Trace Element Behavior

It is convenient to break the variety of elements found in magmatic ores into three groups: the incompatible lithophile elements (see Chapter 13.21), the compatible lithophile elements, and the chalcophile elements (Figure 2). The incompatible lithophile elements are systematically excluded from common rock-forming silicate and oxide minerals during both melting and crystallization, leading to their concentration in melts. The compatible lithophile elements are accommodated in some common rock-forming minerals, leading to their concentration in some magmatic cumulate rocks. The chalcophile elements are those that, like copper, are strongly partitioned into sulfide melts in equilibrium with silicate melts. Since sulfur is a trace constituent of magmas and has a complex geochemistry of its own, the behavior of the chalcophile elements is extremely sensitive to a wide range of intensive parameters and magmatic processes that conspire to dictate the presence or absence of a discrete sulfide phase.

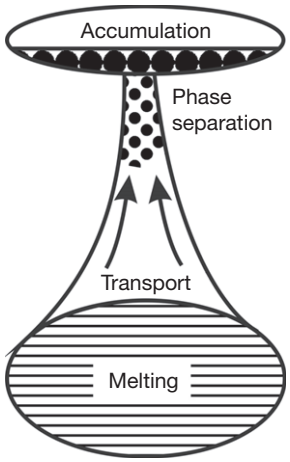

Figure 1 The source–transport–trap model for magmatic ore deposits.

With the sole exception of iron, the ore elements identified in Figure 2 are all trace elements in primary magmas, and their behavior can be described to a first approximation by appealing to the concept of a constant Nernst partition coefficient, which is defined as the concentration of an element in one phase divided by its concentration in another:

$$D_i^{\text{solid/melt}} = \frac{C_i^{\text{solid}}}{C_i^{\text{melt}}} \quad [1]$$

In practice, D may be a complex function of intensive parameters such as oxygen or sulfur fugacity (fO_2 and fS_2) and may depend on the composition of the concentrating phase. However, considerable insight may be gained by treating D as a constant, and here three simple and commonly used expressions are used to describe trace element behavior during individual magmatic processes such as melting, crystallization, or separation of an immiscible melt phase. When n phases coexist, it is necessary to know $n-1$ separate partition coefficients in order to describe the system using any of these expressions. For example, when one is interested in the concentration of an element in a melt phase during partial melting of a polyphase mantle assemblage, the bulk solid/melt partition coefficient D_i^{bulk} is the linear combination of the individual mineral/melt coefficients D_i^p weighted to their proportions in the solid assemblage X^p.

$$D_i^{\text{bulk}} = \sum_{p=1}^{n} D_i^p X^p \quad [2]$$

When rocks melt to form magmas of potential economic interest, large volumes of rock pass through their solidus over timescales that are long in comparison to those of chemical diffusion within individual mineral grains and melt-filled pores. The resulting partially molten magma source region therefore has enough time to attain geochemical equilibrium between coexisting minerals and melts. Although melts may be removed continuously as they form, they tend to migrate great distances through pore networks, continuously reequilibrating with their host rocks before being extracted rapidly along fractures, and consequently the process can be adequately

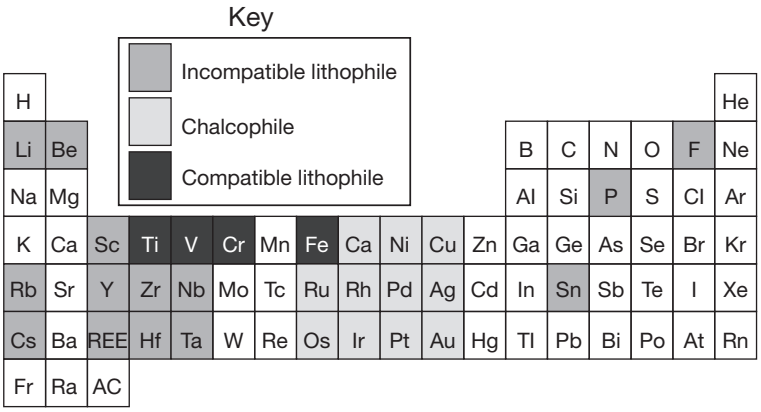

Figure 2 Periodic table showing elements mined from magmatic ores.

described in the present context using the batch equilibrium melting equation:

$$\frac{C_i^{\text{melt}}}{C_i^{\text{bulk}}} = \frac{1}{D_i^{\text{bulk}}(1-F)+F} \quad [3]$$

where C_i^{melt} and C_i^{bulk} are the concentrations of the element i in the melt and in the bulk system, respectively, and F is the weight fraction of the system present as melt.

On the other hand, solids that precipitate from magmas as they travel through the lithosphere tend to be physically separated rapidly from their host magmas, allowing their removal to be treated ideally as fractional crystallization according to:

$$C_i^{\text{melt}} = C_i^{\text{o}} F^{\left(D_i^{\text{bulk}}-1\right)} \quad [4]$$

where C_i^{o} is the concentration of i in the original melt and F is redefined as the weight fraction of melt remaining.

The segregation of sulfide liquids from silicate magmas can be treated as either a batch or a fractional process; the most common approach relies upon the assumption of batch equilibration depending on the ratio R of the mass of coexisting silicate melt over sulfide melt (Campbell and Naldrett, 1979):

$$C_i^{\text{sulfide}} = \frac{C_i^{\text{bulk}} D_i^{\text{sulfide/silicate}}(R+1)}{R + D_i^{\text{sulfide/silicate}}} \quad [5]$$

Equations [3] and [5] are different expressions of exactly the same mathematical relationships, but the entrenched concept of the R factor puts greater emphasis on the critical role played by the interplay between the modal abundance of sulfide and the extreme differences in partition coefficients among the chalcophile elements.

Partition coefficients for the elements in Figure 2 are presented in Table 1 as ranges through which they vary for common assemblages of igneous rock-forming minerals and melts. Also shown are ranges of the partition coefficients for the collector phases commonly responsible for the formation of ore deposits of these elements. For example, vanadium is generally incompatible in mafic silicate magmas lacking magnetite, but once magnetite begins to form, with a $D_V^{\text{magnetite/melt}}$ as high as 50, suitable physical sorting processes might then permit the collection of economic quantities of vanadiferous titanomagnetite. Some of the partition coefficients listed as ranges in Table 1 are known to be functions of fO_2 and other intensive parameters, a matter that is raised again later. A much more extensive set of empirically derived partition coefficients is available from the GERM website (http://earthref.org/GERM/index.html/main.htm). Methods of calculating partition coefficients have also been published (e.g., Blundy and Wood, 2003; Nielsen, 1992; see **Chapter 3.11**).

13.8.3 Fertility of Primary Magmas

A first-order illustration of the effects of melting regimes on trace element abundance in magmas is given in Figure 3. The plot shows the concentrations of several representative elements as a function of the degree of partial melting of a model upper mantle with the composition of the bulk silicate Earth (BSE) (McDonough and Sun, 1995) using partition coefficients from Tables 1 and 2 in eqn [3].

The behavior of niobium has been chosen to represent the incompatible lithophile elements. The silicate melts with the highest niobium concentrations are those resulting from the lowest degrees of partial melting, which in nature would correspond to volatile-rich, alkaline magmas generally formed at great depth below continental lithosphere (e.g., meimechites, alkali picrites, and nephelinites). Progressively greater degrees of melting cause a rapid drop in niobium concentration to the levels commonly observed in tholeiitic suites. The formation of magmatic ore deposits of incompatible lithophile elements is therefore strongly favored by the generation of alkaline magmas from mantle peridotite at very small melt fractions. Subsequent extreme fractional crystallization of niobium-rich alkali basalt may lead to the eventual crystallization of a pyrochlore or loparite cumulate rock from a phonolitic magma. The ultimate enrichment of niobium concentration from the mantle source rock (lower left of Figure 3) to the ore deposit (upper right) spans almost six orders of magnitude.

The case of a compatible lithophile element is illustrated by the curves for chromium in Figure 3. It should be added parenthetically that at the lowest values of F during melting of the mantle, the behavior of chromium is complicated by the

Table 1 Summary of the partitioning behavior of trace elements

Element group	*Examples*	D_i*	*Concentrating phases*	D_i	*Magmatic environments of ore deposition*
Incompatible lithophile	Li, Be, F, Rb, Y, Zr, Nb, Cs, REE, Hf, Ta	<0.1	Melt, rare-element minerals	na	Pegmatite fields Alkaline intrusions Carbonatites
Variable compatibility	P, Ti, V, Cr, Fe	<0.1	Oxide minerals, apatite	10–100	Stratiform intrusions Podiform bodies Immiscible oxide melts
Incompatible chalcophile	Rh, Pt, Pd, Au, Cu	<0.1	Sulfide melt	2000–50 000	Magmatic sulfides
Compatible chalcophile	Os, Ir, Ru, Ni	1–10	Olivine, oxide minerals	500–50 000	Chromitites Magmatic sulfides

D_i* is the bulk partition coefficient between mantle minerals and silicate melt during conditions typical of the generation of basaltic magmas. D_i is the partition coefficient for the phase that ultimately concentrates the element (e.g., sulfide melt for chalcophile elements and oxides for Ti, V, and Cr). Elements with variable compatibility are those that are generally incompatible during melting but that are concentrated in minerals that crystallize from basaltic to intermediate magmas.

Table 2 Preferred values of partition coefficients for chalcophile elements in magmas near 1200 °C and oxygen fugacity near QFM

Cu	*Ni*	*Co*	*Os*	*Ir*	*Ru*	*Rh*	*Pt*	*Pd*	*Au*	*Reference*
Cpx/silicate liquid							1.5			Gaetani and Grove (1997)
Olivine/silicate liquid				2						Brenan et al. (2005)
					2.2	1.9	<0.01	0.01		Brenan et al. (2003)
Spinel/silicate liquid				5–132	1000	75		0.14	0.08	Righter et al. (2004)
Sulfide/silicate liquid	1383	800		14 000				23 000	15 000	Peach et al. (1990)
			30 000	26 000	6400		10 000	17 000	1200	Fleet et al. (1999a)
Mss/sulfide liquid	0.2	0.6–1.5		5	10	4	0.05	0.1	0.005	Mungall et al. (2005)
			4							Brenan (2002)

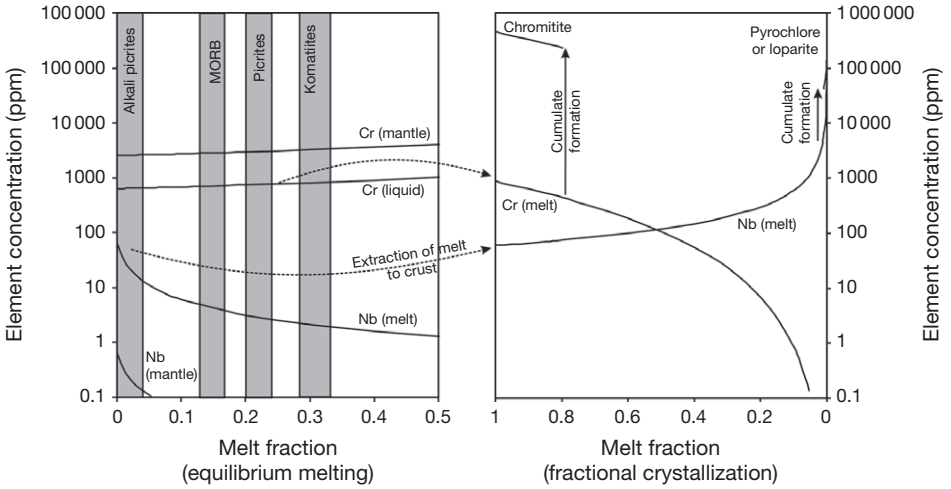

Figure 3 Concentrations of Cr and Nb during melting of the mantle and crystallization of basaltic magmas. Solid curves show compositions of melts. The ranges of the degree of melting required to generate principal magma types are shaded. Dotted curves represent melt extraction events from the mantle (left panel) to the crust (right panel).

possible presence of Cr-spinel and of Cr-rich diopside, which would diminish the chromium concentration in the melt slightly below the values shown. What is important here is that the chromium concentration increases continuously in the melt as the degree of melting increases, although the chromium content of the melt is always less than that of the original source mantle. Magmas produced at the highest degrees of melting have the greatest potential to generate magmatic chromium deposits by the eventual separation of a cumulate rock rich in chromite; in this case, the ore contains only about 100 times the amount of chromium originally present in the mantle source region.

The chalcophile elements present special cases of elements that are highly compatible as long as a sulfide liquid exists in the mantle residue to partial melting, but show either compatible or incompatible behavior in its absence. In the middle panel of Figure 4, the behavior of the platinum group elements (PGE: osmium, iridium, ruthenium, rhodium, platinum, and palladium) and gold is exemplified by plots of palladium, gold, and iridium concentration. The upper mantle is generally thought to contain about 250 ppm of sulfur (McDonough and Sun, 1995). Basaltic melts can dissolve approximately 1000 ppm of sulfide under their typical conditions of formation at oxygen fugacities below that at which quartz, fayalite, and magnetite (QFM) could coexist (i.e., the QFM oxygen buffer). At low degrees of mantle melting, only a small proportion of the sulfur present is dissolved in the basaltic melt, and the remainder is present as a sulfide (i.e., Fe–Ni–Cu–S–O) liquid. As the degree of partial melting increases, the proportion of the total amount of sulfur that is dissolved in the basaltic melt increases until, in this example, at about 25% partial melting, all of the sulfide melt has been dissolved in the silicate melt and no discrete sulfide phase remains in the mantle source. As long as sulfide liquid remains in the restite assemblage, it will sequester the strongly chalcophile elements such as platinum and iridium, leaving them extremely depleted in the coexisting basaltic liquid. As the proportion of sulfide melt decreases to zero, it has a diminishing effect on the total palladium and iridium budget, and the concentrations of these elements rise. After the sulfide melt has been completely dissolved in the basalt, the behavior of the chalcophile elements is controlled only by their partitioning behavior in the remaining restite phases. Palladium, like rhodium, platinum, and gold, is incompatible in silicate phases, so it follows a path to decreasing concentration with increasing melt fraction similar to that shown by niobium. Iridium, which, like osmium and ruthenium, is compatible in olivine, shows a continuous increase in concentration with melting, like chromium. The formation of magmatic ore deposits of the PGE depends first upon the formation of a magma from a source lacking residual sulfide,

which generally requires relatively large degrees of partial melting of the source mantle. Products of extremely high degrees of partial mantle melting are less favorable for generating platinum and palladium deposits than are the picrites formed at about 25% melting.

A growing body of evidence shows that once sulfide liquid has been exhausted by partial melting, the concentrations of some of the PGE in basaltic magmas, notably Ir, Ru, and Os, may be limited by the low-solubility PGE alloy phases that may occur in trace quantities in the restite (e.g., Barnes and Fiorentini, 2008; Borisov and Palme, 2000; Dale et al., 2012).

The behavior of the chalcophile base metals copper and nickel is also illustrated in **Figure 4**. Because these elements have much smaller partition coefficients into sulfide melt than the PGE, they are much less affected by sulfide phase relations. Copper shows a pattern similar to that of platinum, becoming incompatible once the sulfide melt has been consumed, whereas nickel is compatible in olivine, leading to a continuous increase in nickel concentration with continued melting of the mantle source. Magmatic deposits of copper are therefore most likely to form from basaltic magmas resulting from high degrees of partial melting. Nickel concentrations are highest in the largest degree partial melts, leading to the formation of the highest grade nickel deposits from magmas such as komatiites; however, it should be noted that unlike the other chalcophile elements, nickel concentration in basalts is rather insensitive to the presence of residual mantle sulfide. Nickel deposits can, and do, form from magmas sulfide-saturated in their sources, but in these cases, they are unlikely to contain significant amounts of the other chalcophile ore metals copper, platinum, palladium, and gold.

The picture of sulfide phase relations given earlier is appropriate for the melting of upper mantle peridotite under moderate to low oxygen fugacity in the absence of any significant amount of fluid. The presence of even a small amount of volatile elements can depress the silicate solidus (e.g., Katz et al., 2003) into the divariant melting field of monosulfide solid solution (mss) (i.e., magmatic pyrrhotite; Bockrath et al., 2004). Since the iridium-group platinum group elements (IPGE) are compatible in mss, the presence of residual mss in the mantle source of basalt imparts a strong fractionation among the PGE (Bézos et al., 2005). Melting at higher oxygen fugacity than the QFM buffer can cause the early destabilization of mss and sulfide melt and the formation of sulfate, which is much more soluble in silicate melts (Jugo et al., 2005), leading to consumption of sulfide melt, mss, or both even at very low degrees of partial melting (Mungall et al., 2006).

Figure 5 is an element ratio plot showing the compositions plotted in **Figure 4** normalized to the BSE (McDonough and Sun, 1995). The model curve for 30% melting of mantle peridotite closely resembles the compositions of natural komatiites and is representative of the chalcophile element distributions in basaltic magmas that leave their source regions in a state of sulfide undersaturation. The composition of normalmid-ocean ridge basalt (N-MORB) is well duplicated by a model in which 10% of the mantle melts in the presence of 0.1 wt% H_2O. Sulfide remains in the source, sequestering the PGE but having

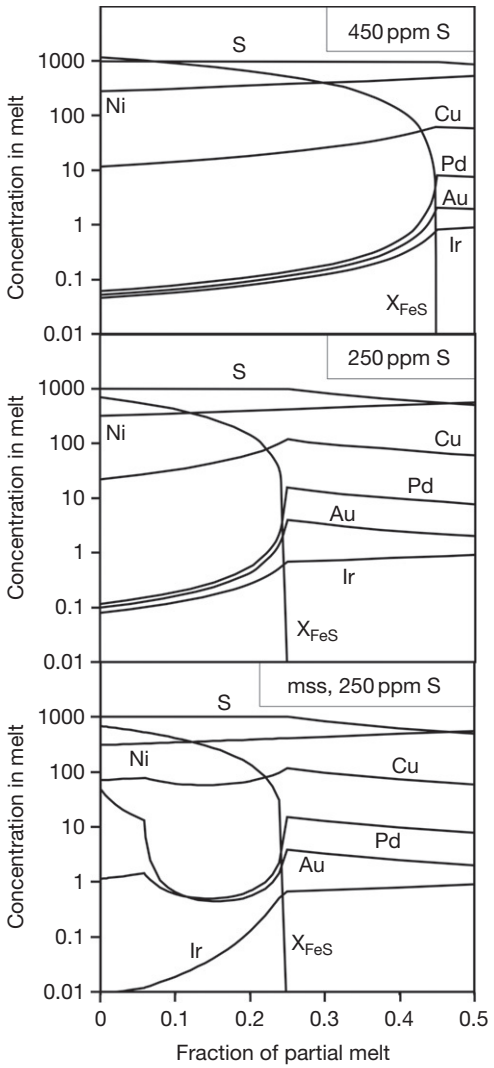

Figure 4 Concentrations of chalcophile elements during melting of the mantle. X_{FeS} denotes the weight fraction (in ppm) of condensed FeS phases in the mantle as melting proceeds. Concentrations of S, Cu, and Ni in the basaltic melt are plotted in ppm. Concentrations of Pd, Au, and Ir are plotted in ppm.

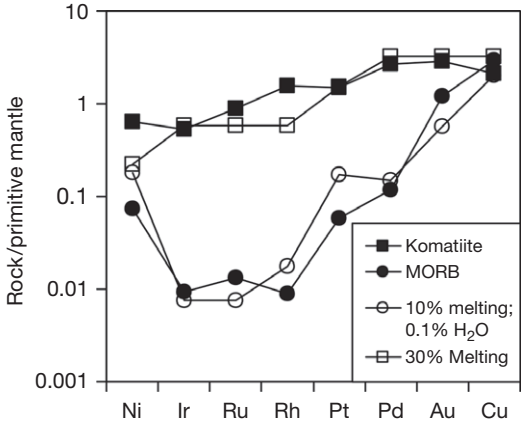

Figure 5 Element ratio plot of chalcophile element concentrations in komatiite and MORB (Crocket, 2002) compared with model results from **Figure 4** (primitive mantle values from McDonough and Sun, 1995).

relatively little effect on the copper and nickel concentrations. The concentrations of iridium, ruthenium, and rhodium are much lower than those of platinum and palladium due to their compatibility in mss.

Highly oxidized alkaline magmas that result from small degrees of partial melting may thus contain sufficiently high chalcophile element concentrations to serve as the progenitors of magmatic ore deposits (Mungall, 2002a; Mungall et al., 2006), but to date, no definitive link has been demonstrated between such magmas and a magmatic ore deposit type. The enigmatic, highly oxidized, iron oxide–copper–gold suite of deposits may represent the hydrothermal products of the crystallization of oxidized calc-alkaline source magmas resulting from the extraction of chalcophile elements from the mantle due to the destabilization of sulfide at high fO_2 during low-degree partial melting.

On the other hand, the introduction of moderately oxidized sulfate-rich fluids to the asthenosphere in suprasubduction zone environments can actually increase the total amount of sulfide in the upper mantle. The top panel of Figure 4 illustrates the dependence of chalcophile element concentrations on the degree of partial melting of a mantle peridotite containing 450 ppm sulfur, as might occur in the mantle wedge of subduction zones due to sulfur fluxing of the slab. Sulfide melt is not fully dissolved in the silicate melt until the mantle has undergone 45% partial melting, which is effectively impossible (Mungall, 2002a). Common arc magmas that owe their existence to the fluxing of the asthenosphere by aqueous fluids are thus unlikely to give rise to significant accumulations of highly chalcophile such as platinum, palladium, and gold.

In summary, the generation of a basaltic magma with high chalcophile element concentrations suitable for later extraction into a sulfide melt to form an ore deposit requires either high degrees of partial melting or small degrees of partial melting at fO_2 above that at which sulfide is predominantly converted to sulfate. To date, all recognized magmatic sulfide deposits apparently owe their origins to large degrees of partial melting of the mantle.

13.8.4 Incompatible Element Deposits

13.8.4.1 Rare-Element Granites, Syenites, and Pegmatites

The existence of magmas unusually rich in incompatible lithophile elements is a necessary but insufficient requirement for the formation of magmatic ore deposits. For example, in Figure 3, the primary low-degree melt contains about 100 ppm niobium, which is a factor of about 1000 below typical ore grades. A secondary process of fractional crystallization must take place to bring the magma to an economic niobium concentration. Inspection of eqn [4] (fractional crystallization) shows that as the melt fraction remaining (F) approaches zero, the concentration of niobium increases toward a singularity. In the present example, assuming that D_{Nb}^{bulk} is approximately zero, eqn [4] predicts that the residual melt would attain ore grade after 99.98% fractional crystallization of the primary melt. What is more likely to occur is that when F is small, the niobium concentration becomes high enough (of order 0.2 wt%) to stabilize a stoichiometric phase of niobium such as pyrochlore or loparite, which may then accumulate from the melt in quantitities sufficient to be mined. For example, the rare earth element (REE) and niobium ores at Lovozero are loparite-rich cumulate layers in a shallowly dipping lopolithic layered felsic alkaline intrusion (Kogarko et al., 2002).

Examples of such extreme fractional crystallization are rare because common alkaline, tholeiitic, and calc-alkaline magmas evolve along Bowen's reaction series to the minima in the system SiO_2–$NaAlSiO_4$–$KAlSiO_4$. They generally lose the geochemical degrees of freedom because of the removal of Ca-plagioclase and ferromagnesian minerals and eventually suffer death by the phase rule at the silica-saturated or silica-undersaturated minima. The solids removed from melts near the eutectics or minima in this system have major element compositions almost identical to the melt composition, so that extreme fractional crystallization could, in principle, take place within a magma chamber whose melt composition changes very little. However, the presence of a eutectic causes the melt to solidify entirely over a very small temperature interval, which interferes with the efficient separation of crystals from residual melt and generally causes the entire magma to freeze in place. To avoid this fate, differentiated felsic magmas must have unusual properties that permit them to retain high geochemical variance and avoid rapid crystallization at a vapor-saturated eutectic. The two main avenues to extreme fractional crystallization of high-variance assemblages involve evolution to either peralkaline or peraluminous residual melts. Progressively greater departures from an alkali–alumina ratio of unity (i.e., molar ratio of (Na + K)/Al) in the presence of important quantities of minor components including fluorine, and in some cases boron, phosphorus, and lithium have the desired effect of either lowering the eutectic temperature or, as described in the following sections, eliminating the eutectic behavior altogether.

Figure 6 schematically illustrates phase relations in the isobaric system $NaAlSi_3O_8$–SiO_2–H_2O (Boettcher and Wyllie, 1969). The presence of K-feldspar and minor ferromagnesian phases in natural magmas would make them harder to represent diagrammatically, but would not change the fundamental principle being illustrated. There is a solvus between hydrous

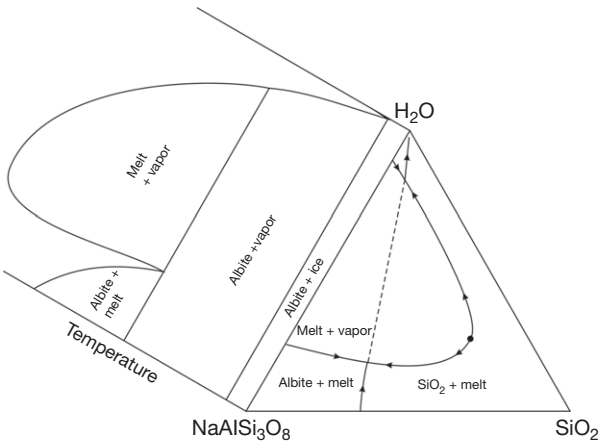

Figure 6 Schematic phase diagram for the system $NaAlSi_3O_8$–SiO_2–H_2O at moderate pressure. After Boettcher AL and Wyllie PJ (1969) Phase relationships in system $NaAlSiO_4$–SiO_2–H_2O to 35 kilobars pressure. *American Journal of Science* 267: 875–909.

granitic melt and silicate-poor aqueous vapor. Crystallization of water-poor granitic melts along the albite–quartz cotectic leads to saturation of the melt in an immiscible aqueous phase at an invariant point. Any amount of further cooling results in complete solidification of the silicate melt to leave an assemblage of solids + vapor, as can be seen schematically in the T–X diagram along the albite–silica join.

At higher pressures, the solvus between hydrous albite melt and aqueous fluid shrinks, and the critical curve at its crest moves to lower temperatures, while the invariant point moves to higher X_{H_2O}. At a pressure near 3.5 GPa, the solvus shrinks to a point as the critical point joins the eutectic; at any pressure above this critical pressure, there is no longer an invariant point and there is no thermodynamic distinction between melt and fluid (at these high pressures, albite is replaced by jadeite but the basic topology remains the same). In this case, as a magma is cooled at its liquidus, the melt evolves continuously to increasingly hydrous compositions without ever encountering an invariant point that would cause it to freeze, until the 'melt' has become a solute-rich aqueous fluid that can migrate away to leave a porous cumulate behind (e.g., Mungall and Martin, 1996). Fractional crystallization can proceed to arbitrarily small melt fractions as the temperature is reduced.

Although the supercritical condition is achieved in the system $NaAlSi_3O_8$–SiO_2–H_2O only at very high pressures, the addition of fluxing components, such as boron, fluorine, or excess Na_2O, to a melt of granitic or phonolitic minimum composition may depress the pressure of the critical point to values at least as low as 4 kbar (Sowerby and Keppler, 2002). Similar processes act on peraluminous melt compositions (London, 1992, 2008). The most extreme example of this behavior is the commonly used cleaning compound known as water glass, which is a hydrous sodium silicate melt that is stable at ambient conditions. Strongly peralkaline magmas are capable of evolving by continuous fractional crystallization without ever reaching a eutectic.

There are two main groups of magmatic ores of incompatible lithophile elements (Cerny, 1992). The NYF group is so named for its abundant niobium, yttrium, and fluorine and generally comprises small hypabyssal plutons of strongly peralkaline silica-saturated or silica-undersaturated felsic rocks. The LCT group is named for its abundant lithium, cesium, and tantalum and comprises peraluminous complexly zoned granitic pegmatites, which tend to appear as swarms of small intrusions emanating from weakly peraluminous leucogranite plutons. In both cases, felsic magmas have been able to evolve to such extremes of fractional crystallization that the liquid itself approaches ore grade for elements usually regarded as trace elements. Once very high concentrations of incompatible elements are achieved, these magmas crystallize a bewildering variety of rare minerals and display unique textures and structures related to their tremendous departure from common silicate melt compositions.

Despite the similarities in the controlling phase relations, peralkaline and peraluminous magmas parental to rare-metal deposits have radically different petrogenesis. The peralkaline magmas are probably derived by extreme fractional crystallization of alkali basaltic magmas produced by small degrees of partial melting of the mantle. The peralkaline condition is achieved by the removal of aluminous phases such as plagioclase and hornblende and exaggerated by the continued removal of alkali feldspar with (Na + K)/Al equal to unity (e.g., Mungall and Martin, 1995). The peraluminous magmas are most likely the products of partial melting of pelitic aluminous metasediments rich in boron, fluorine, and phosphorus under water-undersaturated conditions (London, 1996). In contrast to almost all the other deposit types listed in the following sections, most of which require the liquation (i.e., separation of a liquid into two immiscible liquids) of an immiscible phase, the formation of incompatible element deposits depends on the failure of a magma to do so when normal magmas would.

13.8.4.2 Carbonatite

Carbonatites are igneous rocks composed of more than 50% carbonate minerals, usually spatially and temporally associated with alkaline silicate magmas and having somewhat contentious origins. Although carbonatites make up a vanishingly small proportion of Earth's crust, they account for a large number of the world's very large ore deposits; each newly discovered carbonatite intrusion has approximately a 7% chance of yielding a giant ore deposit (Laznicka, 1999). The principal supplies of REE, niobium, yttrium, P_2O_5, and zirconium are all hosted by carbonatites, which also provide important sources of copper, iron, and scandium.

There are probably three principal varieties of carbonatite: (1) Ca- and Mg-rich carbonate melts formed by melting of carbonate-rich peridotite mantle in the stability field of dolomite. (2) Ca- and Mg- or Na-rich carbonate melts formed by liquation and segregation from CO_2-rich alkaline magmas in the crust (Kjarsgaard, 1998; Lee and Wyllie, 1998; Lee et al., 2000), or (3) calcic carbonatite melts formed by melting of carbonate-rich eclogite in subducted oceanic crust (Hammouda, 2003). It can be difficult to distinguish between a primary mantle derivation and a secondary origin by liquation in the crust as the resulting magmas would be expected to be quite similar and to share a common association with alkaline silicate magmas.

Once formed, carbonate melt will tend to sequester the incompatible elements (e.g., phosphorus, niobium, zirconium, and REE) from coexisting silicate melts or solids, concentrating them and setting the stage for subsequent deposition of rare-element cumulates from the carbonate magma. The crystallization of carbonatite probably proceeds by early removal of calcite from a calcium–magnesian carbonate melt to form calciocarbonatite (Lee et al., 2000). The consequent increase in concentration of iron, magnesium, phosphorus, fluorine, sodium, REE, and niobium, all of which are incompatible in calcite, commonly leads to the eventual crystallization of pyrochlore, apatite, and magnetite from a magnesiocarbonatite magma (e.g., Mitchell and Kjarsgaard, 2004). The solubility of pyrochlore in carbonatite liquid is a sensitive function of the abundance of dissolved species, including F, OH, and P_2O_5 (Mitchell and Kjarsgaard, 2004). Reduction in the concentration of any of these components due to crystallization (e.g., apatite and magnetite) or degassing (e.g., H_2O) may therefore provoke pyrochlore saturation and the formation of a Nb-rich cumulate rock. Continued crystallization results in dolomite saturation and causes continued enrichment in $FeCO_3$ and Na_2CO_3. The ores of the

REE, containing minerals such as monazite and bastnaesite, are associated with dolomitic carbonatite or ferrocarbonatite and may have coexisted with a natrocarbonatite fluid. The aqueous fluids emanating from carbonate melts are saline and rich in incompatible elements, with total concentrations of REE commonly exceeding 3 wt% (Buhn and Rankin, 1999). There is therefore a great potential for the deposition of hydrothermal REE mineralization in the margins of a fundamentally magmatic carbonatite complex.

The high solubility of the rock-forming minerals of carbonatites in deuteric fluids and the ease with which they are recrystallized during metamorphism commonly lead to confusing and contentious field relations reflecting a complex petrogenesis straddling the divide between magmatic and hydrothermal processes (e.g., Bayan Obo; Smith and Henderson, 2000). The tendency for carbonate minerals to dissolve in meteoric water provides an important mechanism for the enrichment of carbonatite ores through the formation of residual soils or redeposited placers rich in oxide or phosphate minerals in supergene environments (e.g., Tomtor; Kravchenko et al., 1996).

13.8.5 Compatible Lithophile Element Deposits

13.8.5.1 Chromitite

Magmatic deposits of chromium are generally essentially monomineralic bodies of chromitite found to be closely associated with mafic or ultramafic silicate rocks. The melting point of chromitite is greater than the liquidus temperature of any recognized terrestrial magma type, making its origin as a Cr-rich oxide liquid very unlikely and favoring its origin as a cumulate from silicate magmas. There are three main types of chromitite: (1) podiform bodies located in the harzburgite mantle tectonite portion of ophiolite complexes, (2) stratiform bodies in layered mafic–ultramafic intrusions, and (3) irregularly stratiform bodies hosted by small ultramafic intrusions. Relatively minor occurrences are also common in the central portions of Ural–Alaskan-type ultramafic complexes (Augé et al., 2005). The presence of large bodies of nearly monomineralic chromite is problematic, considering that the solubility of chromium in basaltic magmas does not usually exceed 2000 ppm.

Podiform chromitites are generally hosted by discordant bodies of dunite, commonly containing pockets of troctolite or other mafic rock. The chromitite–dunite bodies traverse strongly melt-depleted tectonized harzburgite in the uppermost mantle section of ophiolite complexes and are interpreted as the pathways followed by ascending basaltic magmas (e.g., Arai and Matsukage, 1998; Melcher et al., 1999; Zhou and Robinson, 1997; Zhou et al., 1996). A basaltic magma cosaturated with olivine and pyroxene at its source will fall into a state of olivine saturation during ascent and depressurization due to the expansion of the olivine phase volume in the basalt tetrahedron at lower pressure (Herzberg and O'Hara, 1998). The origin of the dunite is ascribed to melt–wall rock reactions involving desilication of orthopyroxene by olivine-saturated basaltic magma. The chromium contained in the orthopyroxene exceeds the carrying capacity of the basaltic melt, leading to the precipitation of Cr-rich spinel along with the dunitic restite to the melt–wall rock reaction. The common presence of an unusual but characteristic suite of minerals as inclusions in the chromite grains, such as albite, orthopyroxene, Na-phlogopite, Ti-amphibole, and rutile (Johan et al., 1983; Melcher et al., 1997), has led many investigators to propose an important role for aqueous fluids in the chromite-precipitating reaction but the details of this process are a matter of ongoing debate, and it is important to recognize that melt inclusions may have suffered partial reequilibration by diffusive exchange with interstitial melt through the enclosing crystals (e.g., Arai and Matsukage, 1998; Matveev and Ballhaus, 2002; Spandler et al., 2005, 2007).

The composition of chromite can be described with a Cr#, defined as the molar ratio Cr/(Cr + Al). There are two main compositional varieties of podiform chromitite. Low-Cr# (40–60) varieties are attributed to the passage of relatively Cr-poor MORB magma through the upper mantle during the initial formation of the ophiolite crust (most likely in a back-arc rift setting). High-Cr# podiform chromitites (70–80) commonly appear in the same ophiolite complex as low-Cr# varieties and are attributed to the passage through the upper mantle of highly magnesian magmas such as boninite. These Cr-rich magmas have highly refractory mantle sources and pass through preexisting oceanic lithosphere in a suprasubduction zone setting shortly before obduction of the host ophiolite sequence.

Stratiform accumulations of chromite up to a meter thick are common in the lower parts of large ultramafic to mafic layered intrusions. Individual layers may be traced for distances of tens to hundreds of kilometers in the largest intrusions, recording processes that occurred simultaneously throughout vast volumes of magma (Kruger, 2005; Scoon and Teigler, 1994). The chromitite commonly appears as a part of a repeated series of cyclic units whose generalized sequence consists of layers of chromitite, dunite, harzburgite, and bronzitite, though in individual units, some of these layers may be missing. There are instances where the sequence evolves upward to norite before returning to chromitite. There are also some examples of concordant, bifurcating chromitite layers hosted by anorthosite (e.g., Nex, 2004), whose origins remain debatable.

Several major chromitite deposits or deposit groups are hosted by relatively small (i.e., kilometer scale) ultramafic intrusions that have served as conduits for komatiitic magmas at shallow crustal levels. In these settings, the chromitite appears as pods or layers that are grossly conformable with igneous layering but whose thickness varies rapidly from centimeter scale to several tens of meters over lateral distances of only a few meters. Examples of this variety include the Sukinda deposits in Orissa state, India (Mondal et al., 2006); the Kemi deposit in Finland (Alapieti et al., 1989); the Ring of Fire deposit group in Ontario, Canada (Mungall et al., 2010); several deposit groups in Zimbabwe (Prendergast, 2008); and the Ipueira–Medrado deposit in Brazil (Marquez and Ferreira, 2003).

There are several factors controlling the solubility of chromite in basaltic liquid. It decreases with falling temperature, with rising fO_2, and with increasing silica content of the melt (e.g., Barnes, 1998). Changes in temperature cannot induce the crystallization of monomineralic layers of chromite from a multiply saturated magma because all cosaturated solid phases will crystallize together as the temperature falls.

Increasing oxygen fugacity has been invoked as a trigger for chromite supersaturation; however, oxygen fugacity cannot be changed simultaneously throughout a body of magma independently of other intensive parameters because it is a function of the activity ratios of coexisting reduced and oxidized melt species such as FeO and Fe_2O_3 – fO_2 is in effect a monitor of a compositional variable and can be changed only by a change in the melt composition. Changes in confining pressure on the order of 20 MPa have been invoked as capable of causing an entire magma chamber to become saturated with chromite alone (Cawthorn, 2005a,b; Lipin, 1993); however, it is difficult to apply this model in cases of chromitite seams several meters thick, such as the 5–8-m-thick main chromitite layer of the Ipueira–Medrado sill, Brazil (Marquez and Ferreira, 2003); or the 60-cm-thick Upper Group 2 (UG2) chromitite of the Bushveld intrusion (e.g., Cawthorn, 2005a,b). In the most extreme examples, considering the limited solubility of Cr in basaltic magmas, mass balance constraints would require extraction of the single chromitite horizon from a magma column as much as 10-km deep. This is clearly impossible in the conduit-hosted deposits such as the Ipueira–Medrado intrusion, which is a sill-shaped intrusion only 7-km long and at present only 300-m thick. In such cases, the chromite must be regarded as a deposit left behind by large volumes of magma as it passed by a fixed point, and the magma 'chamber' is more aptly considered to be a sill-shaped conduit that fed eruption of voluminous basalts higher up.

As illustrated in **Figure 7** (after Irvine, 1975, 1977), there are a number of scenarios involving magma mixing or the assimilation of silica-rich host rocks that can provoke a magma to become saturated solely with chromite. A mafic magma at point L_1 forms dunitic cumulates until the residual melt reaches the chromite–olivine cotectic, whereupon a small amount of chromite begins to crystallize with the olivine. Continued cooling causes the melt to evolve to the distribution point *D*, where olivine and chromite are simultaneously in a peritectic relationship with Cr-rich orthopyroxene. Removal of orthopyroxene (and possibly also plagioclase) causes the deposition of orthopyroxenite or norite cumulate rocks. If any two consanguineous magmas along the path from L_2 to L_3 are mixed by subsequent injections of new magma into a magma chamber, the resulting melt is likely to fall in the chromite field. A monomineralic layer of chromite will form until the melt has returned to the olivine–chromite cotectic. Other scenarios are possible. For example, addition of silica to L_2 will drive the hybrid melt into the chromite-only divariant field. Silica addition might result from the assimilation of wall rocks or from the injection of a buoyant plume of mafic magma into a stratified magma chamber having a felsic liquid capping layer. Another means of producing chromite in **Figure 7** is partial melting, by addition of deuteric fluxes of H_2O, harzburgite, orthopyroxenite, or norite orthocumulate rocks. If such rocks lack significant amounts of trapped liquid (i.e., they lack interstitial quartz), they will begin to melt at the peritectic point *D*. Since liquids at *D* contain considerably less chromium than the orthopyroxene that is melting, the residue must contain chromite. Such relations may control the formation of narrow chromitite selvages mantling zones of remelted pegmatitic norite in the Bushveld intrusion (Nicholson and Mathez, 1991). Similar melting relations involving the desilication of mantle orthopyroxene are likely to play an important role in promoting chromite growth in podiform chromitites.

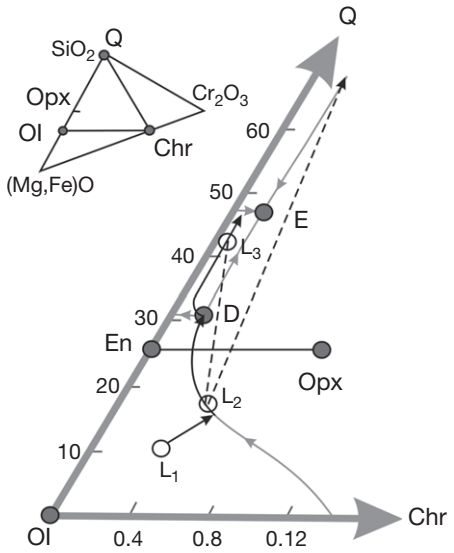

Figure 7 Portion of the system Mg_2SiO_4–$MgCr_2O_4$–SiO_2. Solid gray lines indicate cotectic or peritectic reactions; dashed lines indicate mixing lines. Reproduced with permission from Irvine TN (1975) Crystallization sequences in the Muskox intrusion and other layered intrusions. II. Origin of chromitite layers and similar deposits of other magmatic ores. *Geochimica et Cosmochimica* Acta 39: 991–1008; Irvine TN (1977) Origin of chromitite layers in the Muskox intrusion and other stratiform intrusions: A new interpretation. *Geology* 5: 273–277.

The intensive parameters causing chromite to become the sole liquidus phase in a magma therefore must be some combination of changes in composition. The simultaneous deposition of monomineralic layers of chromitite on the bases of magma chambers must result from a simultaneous change in magma composition within a layer of melt extending laterally throughout the magma chamber, whether the actual trigger is changing fO_2, silica content, H_2O content, or some other compositional parameter. Wholesale changes in melt composition can be achieved by mixing events, wherein a fluid or melt is discharged into the magma and mixes turbulently with the magma, or when buoyant new influxes of primitive magma reach the felsic liquid at the top of a magma chamber (Irvine, 1975, 1977; Kinnaird et al., 2002; Li et al., 2005; Naldrett et al., 2009a; Spandler et al., 2005). Since liquids flow laterally to achieve a level of neutral buoyancy, this process will tend to be felt over the entire width of a magma body over the timescale of melt migration, which is much shorter than the timescale of magmatic differentiation and will therefore appear as an instantaneous event in the layered stratigraphy of the intrusion. In a closely related hypothesis, chromite may accumulate in large quantities in a magmatic feeder system prior to its injection into a magma body as a slurry, whereupon suspended chromite crystals may travel great distances along the base of the magma chamber before settling to form layers (Mondal and Mathez, 2007). Similarly, in settings such as the conduit-hosted chromitite deposits, hydraulic sorting of chromite and olivine by flowing magma may be sufficient to produce chromite bodies and dunite bodies from masses of suspended or

saltating crystals in which the chromite and olivine originally coexisted in cotectic proportions. Given the variety of possible causes of chromite saturation, it is likely that chromitite horizons in layered intrusions have formed in response to all these causes at different times, possibly forming by different mechanisms at different levels within single layered intrusions.

As a parting comment about chromitite, it is intriguing to note that whereas bizarre mineral or melt inclusions observed in podiform chromitites are attributed to fluid–mantle interactions, identical inclusions are attributed to a completely different process of magma mixing when they are observed in stratiform chromitites. Given the similarity of the two sets of inclusions, it may be that neither hypothesis adequately accounts for the presence of this very unusual suite of mineral and melt inclusions (see **Chapter 13.6**).

13.8.5.2 Stratiform Magnetitite

Large mafic layered intrusions commonly possess monomineralic magnetite layers up to several meters thick at higher levels in the stratigraphy than the chromitites (Reynolds, 1985; Zhou et al., 2005). The magnetite may be rich in Ti and V and, in some instances, can be exploited as a polymetallic Fe–Ti–V deposit. The magnetitite horizons form from Fe–Ti-rich highly evolved basaltic melts late in the evolution of the layered intrusion. In the Bushveld intrusion, the gabbroic cumulate rocks below the first magnetite horizon show a gradual increase in the amount of intercumulus magnetite, perhaps indicating that the melt from which they formed was increasingly close to magnetite saturation. Above the first magnetitite horizon, magnetite remains in the cumulus assemblage. The compositions of magnetite crystals in the magnetitite horizons are broadly similar to those of the cumulus or interstitial magnetite in the intervening mafic silicate cumulates. There are minor cyclical changes in the trace element content of the magnetite (e.g., increase in chromium) at each magnetitite horizon, possibly reflecting a recharge of melt or fluid at the time of each magnetitite depositional event. The magnetitite horizons in at least some instances coincide with the tops of discordant iron-rich ultramafic pegmatitic pipe structures in the underlying cumulate piles. These ultramafic pegmatites can be interpreted as drainage channels for dense highly fractionated Fe-rich melt down into the cumulate pile (Reid and Basson, 2002; Scoon and Eales, 2002; Scoon and Mitchell, 2004).

The controls on magnetite solubility in mafic liquids are, like those for chromite, predominantly compositional. Increasing fO_2 decreases magnetite solubility, whereas the addition of H_2O to a melt can suppress silicate crystallization while permitting continued magnetite crystallization. Interactions between melts of differing compositions within complexly stratified magma sheets, analogous to the ones illustrated for the chromite case in **Figure 7**, could explain the sudden change from deposition of magnetite gabbro to magnetitite (e.g., Tegner et al., 2006).

Another hypothesis for the origins of the cumulus oxide deposits involves the separation of highly evolved Fe–Ti-rich basaltic magmas (i.e., ferrobasalts) into a pair of immiscible silicate liquids, one of which is very rich in iron, titanium, vanadium, zirconium, manganese, and other high field-strength cations but poor in SiO_2 and alkalies, the other being complementarily enriched in alkalies and silica. Immiscibility across this solvus has been well documented experimentally (McBirney and Nakamura, 1974; Naslund, 1983) and has also been convincingly demonstrated in the Skaergaard intrusion through observations of coexisting melt inclusions hosted by apatite (Jakobsen et al., 2005). Proponents of the immiscibility hypothesis suggest that ferrobasaltic magma undergoes phase separation, with the denser Fe-rich melt then ponding at the base of the magma chamber or even percolating down into the upper part of the cumulate pile. As the Fe-rich silicate liquid then crystallizes, it will leave Fe–Ti oxides (Ti magnetite or ilmenite) either as monomineralic layers concordant with layering (Reynolds, 1985), as downward-stepping sills and dikes cutting the previously formed silicate cumulates (Ripley et al., 1998), or as poikilitic or net-textured oxide accumulations surrounding previously formed cumulus silicates (Zhou et al., 2005).

The value of magnetitites as ore deposits stems in large part from their extraordinary vanadium and titanium contents. Both of these elements are incompatible throughout the melting and subsequent fractional crystallization history of the basaltic magma, until the point at which the first Fe oxide mineral reaches the liquidus. At this point, both titanium and vanadium switch from being incompatible to compatible, permitting their efficient removal from the magma within magnetite or ilmenite accumulates.

Vanadium is strongly depleted in the melt by its removal into the early formed magnetite because D_V is very large in magnetite, of order 50. The partition coefficient for vanadium into magnetite and other liquidus phases is a sensitive function of fO_2 because it exists as both V^{3+} and V^{5+} states in the melt (Toplis and Corgne, 2002). Only V^{3+} is easily accommodated in oxide minerals, so that as fO_2 increases and V^{5+} increases in abundance, the D_V decreases. The D_V for ilmenite is generally smaller than that for magnetite, so early ilmenite crystallization will tend to deplete the melt in vanadium without concentrating vanadium sufficiently to form an economic deposit. Higher fO_2 favors the early crystallization of magnetite rather than ilmenite (Toplis and Corgne, 2002) but also diminishes D_V. Formation of magnetitite ores is therefore favored in magmas with relatively low titanium due to their origin by large degrees of partial melting, and with moderate to low fO_2 to enhance the segregation of vanadium into early forming magnetite. The depletion of vanadium in the magma by magnetite crystallization makes later magnetite horizons uneconomic; it is generally the first thick magnetitite in a layered intrusion that will contain the vanadium deposit, if one is to be found at all.

13.8.5.3 Kiruna-Type Ores and Nelsonites

There are a number of occurrences worldwide of magnetitite that have been widely interpreted to have formed by solidification of a P_2O_5-rich Fe oxide magma. Intrusive magnetite–apatite bodies termed nelsonites have attracted attention as curiosities (Kolker, 1982); however, the most important deposits in this class are relatively poor in apatite but may have accessory Fe phosphate minerals. The most notable examples are volcanic rocks on the El Laco volcano in Chile and their ancient equivalents at Kiruna in Sweden (Nystrom and Henriquez, 1994). The quantities of magnetite involved are considerable, with tonnages in the range of 500 Mt being

common. Critical pieces of evidence in favor of a magmatic origin for these rocks include the presence of delicately preserved pyroclastic textures such as bombs, ash-flow tuffs, and bomb sags in unconsolidated pyroclastic materials composed entirely of hematite, magnetite, and iron phosphate minerals. Lavas now composed of iron oxides preserve vesicles, fluid escape structures, chilled margins, and all the textural features expected of fresh lava flows, while also having columnar and dendritic mineral textures identical to those found in synthetic Fe oxide slags (Henriquez and Nystrom, 1998; Nystrom and Henriquez, 1994). The magnetite is commonly coated with Fe phosphate and contains accessory apatite and diopside or tremolite. Around the margins of the lava flows, there has been abundant and intense hydrothermal alteration, evidenced by wholesale replacement of dacitic and andesitic lavas and pyroclastic rocks by scapolite, diopside, and magnetite. The marginal alteration textures have been interpreted by some workers as evidence that the entire magnetite bodies may indeed be replacements of preexisting silicate lava flows by magnetite (Sillitoe and Burrows, 2002). The main obstacles to the acceptance of this hypothesis are (1) textures that faithfully reproduce not only the large-scale textures of the lavas but also the empty vesicles and empty pore spaces within still-unconsolidated oxide pyroclastic deposits (Henriquez and Nystrom, 1998) and (2) the presence of fluid inclusions in the flows that were trapped at magmatic temperatures (Broman et al., 1999) and could not have resulted from trapping of shallow epithermal fluids as proposed by Sillitoe and Burrows (2002).

The origins of iron oxide magmas have been controversial, but increasing evidence exists to support an origin through the breakdown of oxidized intermediate silicate magmas into a pair of immiscible melts. Philpotts (1967) demonstrated experimentally in a simple synthetic analog system that P-rich Fe oxide liquid could coexist with Fe-poor silicic melt. Clark and Kontak (2004) have shown that magma mixing in a highly oxidized potassic calc-alkaline volcanic system has led to the separation of some hybrid melts into two immiscible liquids. One has a highly silicic rhyolitic composition, whereas the other has widely variable but very FeO-rich composition. Similar immiscible oxide–silicate melt pairs have been observed to be coexisting in melt–fluid inclusions in quartz phenocrysts in highly silicic ignimbrites (Naumov et al., 1993).

Glass-forming melts composed of Fe oxides and Fe phosphate have been proposed as nuclear waste storage media because they remain molten well below 1000 °C and are ideal fluxes for a wide variety of other compounds (e.g., Karabulut et al., 2002).

Weidner (1982) documented an invariant point in the system Fe–C–O at 815 °C and 0.3 kbar where magnetite, wüstite, graphite, liquid, and vapor coexist. The magnetite–graphite–liquid–vapor univariant reaction, corresponding to the solidus curve for an iron oxide liquid, rises from this invariant point and remains at reasonably low pressures over a wide range of temperatures, indicating that iron oxide liquids are stable in Earth's crust at moderate pressure in the range of temperatures and oxygen fugacities typical of terrestrial magmas. The convergence of experimental and field evidence suggests that Fe oxide ore liquids can indeed form in nature, and that the textural evidence for their existence should be taken at face value.

13.8.5.4 Tellnes-Type Ti Deposits

There are several examples of apparently intrusive masses of ilmenite associated with anorthositic massifs (e.g., Tellnes, Norway; Lac Tio, Quebec; Ilmen Mountains, Russia; Force, 1991). These bodies may exceed 300 Mt and show a variety of structural and textural forms. There are clearly discordant bodies resembling dikes and sills, with xenoliths and vein-like apophyses; there are also lenticular or equidimensional masses as well as very extensive concordant layers that apparently form part of the magmatic stratigraphy. There is as yet little petrogenetic evidence to shed light on the origins of these rocks, but their intrusive forms suggest that they are similar in origin to the Ti-magnetite deposits described earlier.

13.8.6 Magmatic Chalcophile Element Deposits

13.8.6.1 Sulfide Liquid Immiscibility

With very few exceptions, magmatic deposits of the chalcophile elements represent primary accumulations of immiscible sulfide liquid within a silicate magma. There are many different structural settings in which this may occur, and a detailed discussion of them would be beyond the scope of this review.

The fundamental control on the deposition of magmatic sulfides is the solubility of sulfide in silicate melts. Once sulfide melt is present, the distribution of chalcophile elements between silicate and sulfide melts is a sensitive function of the magnitude of the partition coefficients and of the modal abundance of sulfide in the system. Due to the extraordinarily large partition coefficients for the PGE, the presence of even a fraction of a percent of sulfide in a silicate magma can quantitatively strip it of its PGE, forming a very high tenor sulfide melt and a completely impoverished silicate.

13.8.6.2 Sulfide Solubility

The solubility of sulfide ions in silicate melt can be understood as resulting from the replacement of oxygen on the anion sublattice of the melt by S^{2-} ions, predominantly in the neighborhood of Fe^{2+} cations (Fincham and Richardson, 1954). The exchange reaction

$$FeO_{sil} + {}^1/_2\,S_2 = FeS_{sil} + {}^1/_2O_2 \quad K_6 \qquad [6]$$

expresses this process and illustrates the dependence of the activity of dissolved S (as FeS) on both oxygen and sulfur fugacity. The equilibrium constant can be combined with the activity coefficients for the dissolved melt species and rearranged to yield a parameter called the sulfide capacity, C_S, that is defined by the following relation:

$$X^{sil}_{FeS} = K_6\gamma^{sil}_{FeS}a^{sil}_{FeO}\left(\frac{fS_2}{fO_2}\right)^{1/2} = C_S\left(\frac{fS_2}{fO_2}\right)^{1/2} \qquad [7]$$

The concept of sulfide capacity has been tested by several investigators and found to be an excellent predictor of the solubility of sulfide in melts equilibrated with a gas stream containing controlled fO_2 and fS_2 (O'Neill and Mavrogenes, 2002). Sulfide capacity is a strong function of melt composition,

showing positive correlations with concentrations of FeO and TiO_2 and negative correlations with concentrations of SiO_2 and Al_2O_3; by far the greatest contribution is made by FeO.

When the silicate melt is in equilibrium with a sulfide melt of approximately FeS composition, the exchange reaction

$$FeO_{sil} + {}^1/_2\, S_2 = FeS_{sul} + {}^1/_2\, O_2 \qquad [8]$$

can be combined with eqn [6] to yield a simple reaction

$$FeS_{sil} = FeS_{sul} \qquad [9]$$

that does not explicitly involve either sulfur or oxygen. Equation [9] suggests that, to a first approximation, the sulfur concentration at sulfide saturation (SCSS) in the silicate melt does not depend on fO_2 or fS_2. However, the relation expressed by eqn [6] still applies; in other words, when silicate and sulfide melt coexist at equilibrium, the fugacities of sulfur and oxygen cannot vary independently of each other. Since fO_2 tends to be held within narrow bounds by the homogeneous equilibrium between FeO and Fe_2O_3, which are major components of the melt, the fS_2 is effectively buffered by the presence of sulfide melt at a given fO_2. If the FeO content of a sulfide-saturated melt changes, so too do fO_2 and fS_2. The SCSS in a silicate melt at a given fS_2 or fO_2 does depend explicitly on the sulfide capacity, according to the following relation:

$$\ln [S]_{SCSS} = \frac{\Delta G^\circ(8)}{RT} + \ln C_S + \ln a^{sul}_{FeS} - \ln a^{sil}_{FeO} \qquad [10]$$

where $\Delta G^\circ(8)$ is the free energy of reaction of eqn [8] and T is measured in kelvin.

The SCSS shows second-order dependencies on fO_2 and fS_2 through their controls on such parameters as the ratio of FeO to Fe_2O_3 in both melts. The activity of FeS in sulfide melt will diminish to the extent that it is diluted by the base metal sulfides CuS and NiS. The SCSS depends on melt composition through the sulfide capacity and the concentration of FeO and has been found to diminish with increasing pressure and decreasing temperature, as reviewed and summarized empirically by Li and Ripley (2009).

A more elaborate thermodynamic model applicable to magmas ranging from mafic to felsic in composition was presented by Moretti and Ottonello (2005) and Moretti and Baker (2008); however, for simple modeling of mafic systems, the Li and Ripley (2009) model is adequate.

Whether a basaltic silicate magma forms in the presence of sulfide liquid or not, it will become sulfide undersaturated as it rises into the mantle lithosphere and crust because of the decrease in pressure (Mavrogenes and O'Neill, 1999). Basaltic magmas therefore arrive in the crust in a state of sulfide undersaturation containing approximately 1000 ppm sulfur and will not precipitate a sulfide liquid unless provoked to do so by external factors.

13.8.6.3 Chalcophile Element Partitioning

The distribution of trace elements between silicate and sulfide melts can be written in forms similar to eqns [6] and [8]. If the element in question is dissolved in the silicate melt as an oxide species such as PtO (to represent the PGE in general), the exchange reaction is as follows:

$$PtO_{sil} + {}^1/_2S_2 = PtS_{sul} + {}^1/_2O_2 \qquad K_9 \qquad [11]$$

and the partition coefficient can be expressed as

$$D^{sul/sil}_{Pt} = K_9 \frac{\gamma^{sil}_{PtO}}{\gamma^{sul}_{PtS}} \left(\frac{fS_2}{fO_2}\right)^{1/2} \qquad [12]$$

which shows an explicit dependence on the oxygen and sulfur fugacities. According to eqn [7], a given melt with its compositionally dependent SCSS and C_S will equilibrate with sulfide melt at a fixed fO_2/fS_2 ratio. However, different silicate melts have different sulfide capacities and different SCSS, which are capable of varying independently and therefore permit silicate and sulfide melt to coexist over a wide range of fO_2/fS_2 ratios. It is therefore inevitable that $D^{sul/sil}_{Pt}$ will be a function of silicate melt composition, temperature, and pressure. Comparing eqns [7] and [12], one can infer that the sulfide/silicate partition coefficients of the PGE should be much smaller in Fe-poor systems such as dacites and rhyolites than they are in mafic and ultramafic magmas (Brenan, 2008). To the extent that a metal is associated with sulfur in the silicate melt, as is known to be the case for iron, the concentration of that metal in the silicate can be increased beyond the concentration that eqn [11] would predict, in a manner analogous to the increase in total metal concentration in an aqueous fluid when several complexes of the same metal coexist. Since sulfur concentrations are not much higher than base metal concentrations in typical magma, this effect is less likely to control partitioning of the base metals than the PGE, which are present at concentrations a hundred times less than that of sulfur. Partition coefficients for the base metals have been measured in a range of conditions and shown to obey relations similar to those expressed in eqn [11] (see **Table 3**). Data describing partitioning of PGE between silicate and sulfide melts are too sparse to permit such detailed models of their dependence on intensive parameters (**Tables 2** and **3**). The data available indicate that sulfide/silicate melt partition coefficients for PGE are extremely large, of similar magnitude for all of the PGE, and seem to increase with increasing fO_2 of equilibration. Since the most oxidized experimental condition published was at the Fe–FeO oxygen buffer, it is likely that the partition coefficients for PGE in natural basaltic magmas are larger than the measured values shown, probably in the neighborhood of 50 000.

13.8.6.4 Sulfide Segregation

Much has been written about the geochemical process of the segregation of immiscible sulfide liquids from basaltic magmas since the classic description by Campbell and Naldrett (1979). For example, Li and Ripley (2009) and Naldrett et al. (2009a, b) have examined the path to sulfide saturation in the Bushveld complex, which hosts the world's largest accumulation of Pt-rich sulfide ore. The classic example of a magmatic Ni–Cu–PGE sulfide deposit is the Siberian trap flood basalt province, where a thick succession of tholeiitic basalts show notable PGE depletions that have been attributed to the removal of sulfide in the feeder conduit in which the massive

sulfide deposits of the Noril'sk–Talnakh camp were formed (e.g., Arndt et al., 2003; Brugmann et al., 1993; Czamanske et al., 1995; Li et al., 2009; Lightfoot and Keays, 2005). Several of these papers have described detailed geochemical models of the process of magma evolution and sulfide segregation at Noril'sk. The intricate details of this process remain controversial, and it is not the purpose of this chapter to examine all competing viewpoints. Instead, selected data from Noril'sk are compared with the results of a series of simple models of magma evolution in a purely illustrative sense to demonstrate some ways in which magmas can become saturated with sulfide liquid.

Sediment assimilation and equilibrium crystallization of a magnesian tholeiitic basalt magma were calculated using the thermodynamic modeling program PELE (Boudreau, 1999b). The resulting variations in trace element concentrations appear in Figure 8 as functions of the temperature of the system as it cools and assimilates. The parent magma chosen is the most magnesian tholeiitic member of the Tuklonsky Formation of the Siberian traps (1f29; Lightfoot et al., 1993), which is selected as a reasonable choice for a primitive mantle-derived magma from which the massive Noril'sk–Talnakh ore deposits were extracted after interactions with the crust produced contaminated flood basalts such as the Nadezhdinsky and Morongovsky formations. Although there are more magnesian picrites in the same formation, these are most likely samples of basalt (with the composition of sample 1f29) into which some

Table 3 Parameterizations of partition coefficients for chalcophile elements in sulfide phases

Parameterization	*Reference*
Partition coefficients $D_M^{sul/sil}$ (sulfide melt/silicate melt) for base and precious metals	
$\log\left(D_{Cu}^{sul/sil}\right) = 0.38\frac{\log(fS_2)^{1/2}}{\log(fO_2)^{1/2}} + 1.27$	Gaetani and Grove (1997)
$\log\left(D_{Ni}^{sul/sil}\right) = 0.60\frac{\log(fS_2)^{1/2}}{\log(fO_2)^{1/2}} + 1.40$	Peach and Mathez (1993)
$\log\left(D_{Co}^{sul/sil}\right) = 0.69\frac{\log(fS_2)^{1/2}}{\log(fO_2)^{1/2}} - 0.88$	Gaetani and Grove (1997)
$\log\left(D_{Cu}^{sul/sil}\right) = 0.2548\frac{\log(fS_2)^{1/2}}{\log(fO_2)^{1/2}} + 1.9501$	Ripley et al. (2002)
Partition coefficients $D_M^{mss/liq}$ for PGE. S+O in the sulfide liquid is expressed in mol%	
$\log(D_{Au}) = 0.0021(S+O) - 2.2551$	Mungall (2005)
$\log(D_{Ir}) = 0.0201(S+O) - 0.2658$	Mungall (2005)
$\log(D_{Ru}) = -0.0758(S+O) + 4.644$	Mungall (2005)
$\log(D_{Rh}) = 0.0390(S+O) - 1.449$	Mungall (2005)
$\log(D_{Pt}) = 0.1523(S+O) - 8.6063$	Mungall (2005)
$\log(D_{Pd}) = 0.0837(S+O) - 5.0498$	Mungall (2005)

Partitioning of Ni and Cu between mss and sulfide melt at low pressure. The sulfide melt composition is expressed in mol% of Ni, Cu, Fe, S*, where S* is the sum of the two anions S and O. The mss composition is expressed in mol% of the components FeS, NiS, CuS, and ·S where ·S represents a cation vacancy in mss. K_Ds are defined as follows (Mungall, 2007):

$$\log K_D^{Cu} = \frac{-600}{T} + 2.5X_l^{S^*} - 0.85 = \log\frac{X_s^{CuS}}{X_l^{Cu}X_l^{S^*}} = \log X_s^{CuS} - \log X_l^{Cu} - \log X_l^{S^*}$$

$$\log K_D^{Ni} = \frac{4500}{T} + 4.2X_l^{S^*} - 5.1 = \log\frac{X_s^{NiS}}{X_l^{Ni}X_l^{S^*}} \log X_s^{NiS} - \log X_l^{Ni} - \log X_l^{S^*}$$

$$\log K_D^{S} = \frac{3000}{T} + 9X_l^{S^*} - 7.6 = \log\frac{X_s^{\bullet S}}{X_l^{S^*}} = \log X_s^{\bullet S} - \log X_l^{S^*}$$

T is measured in kelvin.

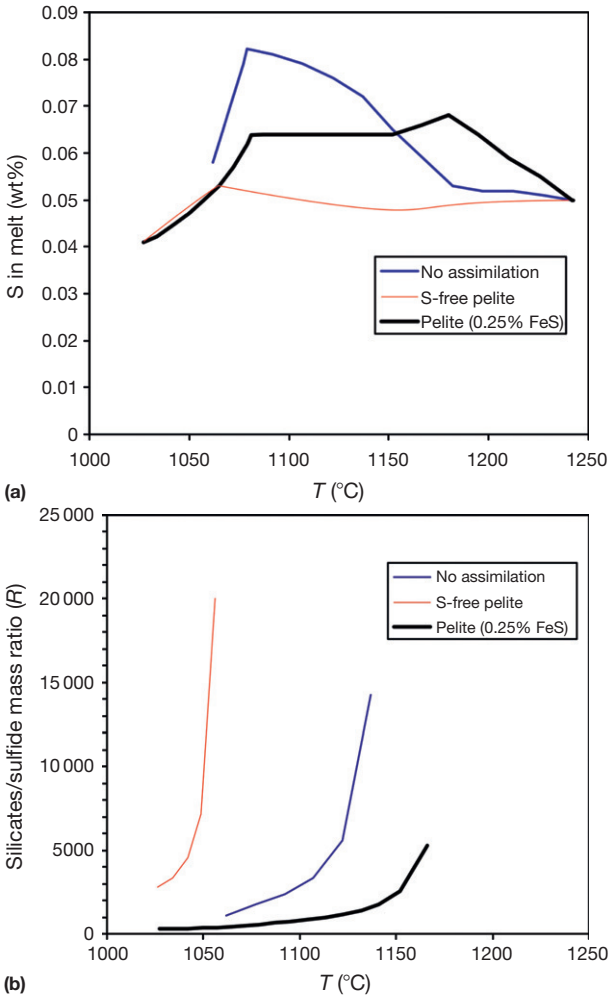

Figure 8 Consequences of sulfide saturation in model Siberian trap magma. (a) Modeled concentration of S during equilibrium crystallization or during isenthalpic assimilation of pelitic sediment containing either no sulfur or 0.25 wt% FeS. (b) Silicate/sulfide mass ratio (R) after sulfide saturation. (c) Concentrations of Pt and Cu in sulfide melt at equilibrium with basalt. Dashed curves show Cu concentrations in weight percent (right-hand scale), whereas solid curves show Pt concentration in ppm (left-hand scale). Assimilation of any more than a very small fraction of sulfide-rich sediment dilutes the metal content of the sulfide to low values. Extremely PGE-rich sulfide ores such as those at Noril'sk probably result from the assimilation of S-poor or S-free rocks. (d) Concentrations of Pd and Zr in lavas from the Siberian traps, compared with the results of the models shown in parts (a), (b), and (c). The very low Pd concentrations in the Nadezhdinsky lavas reflect equilibration with sulfide at a low silicate/sulfide mass ratio. (e) Variation of the ratio of Cu/Pd in Siberian traps compared with model results. Most lavas lie along a trend of constant Cu/Pd, reflecting no history of equilibration with sulfide liquid. Some Nadezhdinsky lavas show even more extreme values of Cu/Pd than the most depleted model trend, indicating equilibration at even lower silicate/sulfide mass ratios than the minimum model values of about 400.

(Continued)

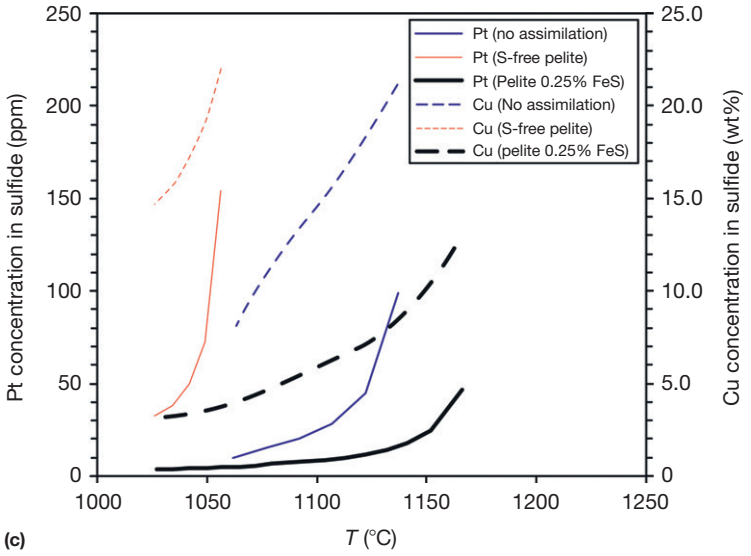

(c)

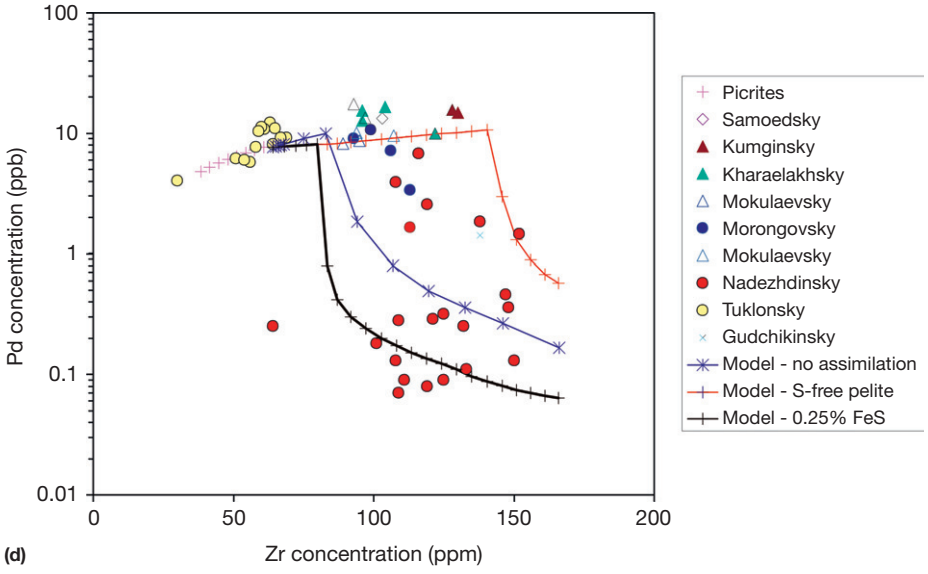

(d)

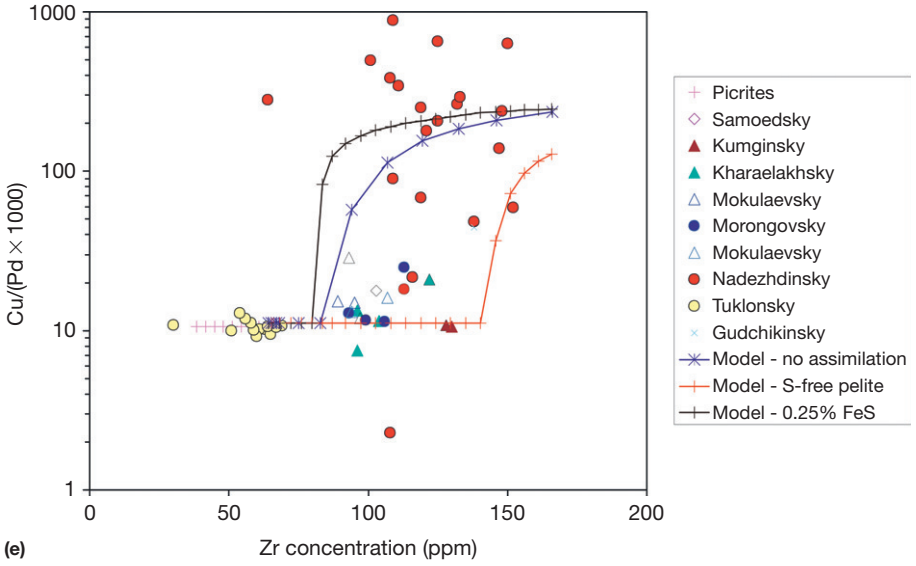

(e)

Figure 8 (Continued)

quantity of olivine has accumulated. In any case, the difference is not critical to the discussion that follows.

The model was run for three different scenarios. These three scenarios were chosen to contrast the effects of closed-system crystallization as might occur in a large magma chamber, or of wholesale assimilation of crustal rocks as might occur in a magmatic conduit in the crust. It is important to stress that despite the illustrative choice of magma compositions from Noril'sk, the present model is intended to demonstrate general principles rather than to solve the petrogenesis of the Noril'sk deposits in particular. In the first scenario, the basalt (assumed to contain 500 ppm sulfur) was allowed to cool and crystallize without any addition or subtraction of materials. In another, the basalt was allowed isenthalpically to assimilate a pelitic metasediment (trace element abundances of average post-Archean pelite of Gao et al. (1998)) and the compositions of the resulting cumulates and liquid were calculated. In the third model, various amounts of pelite identical to the previous one but containing 0.25 wt% of FeS were assimilated. The calculations were conducted assuming equilibrium between all phases rather than using a fractional segregation process, so the plots represent the locus of all the possible final states of systems equilibrated internally for a given amount of added pelite, rather than a path followed by an individual system during a dynamic process of assimilation and fractional crystallization. **Figure 8(a)** shows the concentrations of sulfur in basalts resulting from different extents of equilibrium crystallization (labeled 'no assimilation') or from different extents of assimilation of pelite.

During crystallization, sulfide is incompatible, so its concentration will rise in the melt at the same time as sulfide solubility is being diminished by falling temperature. This effect will be delayed somewhat if the magma evolves along a trend toward iron enrichment, but once iron depletion begins, the solubility of sulfide will drop rapidly. It is therefore possible for a basaltic magma to undergo a considerable amount of crystallization in a state of sulfide undersaturation before it begins to precipitate droplets of sulfide liquid.

If the same magma encounters easily fusible metasediments, then it will suffer a more rapid drop in sulfide solubility as it assimilates SiO_2 and Al_2O_3. However, the sediment is an efficient flux, so that the quantity of liquid does not change much until a large amount of sediment has been added; instead, a mass of olivine-rich cumulates will form that is approximately equal to the mass of sediment assimilated. The primitive tholeiitic magma can absorb about half of its original weight in sediments in this manner without losing much mass. The concentration of sulfur in the melt consequently does not change much at first. When larger amounts of crystallization occur, the contaminated basaltic melt will eventually become sulfide saturated at a sulfur concentration lower than that at which the uncontaminated basalt would do (**Figure 8(a)**). On the other hand, if the metasediment contains an appreciable amount of sulfide minerals, the quantity of sulfide in the magma after assimilation can easily exceed the solubility of sulfide in the silicate melt, leading to a gross sulfide oversaturation after relatively small amounts of assimilation.

The three different paths to sulfide saturation result in the liquation of sulfide melt with very different compositions due to the importance of the modal abundance of sulfide (or degree of sulfide supersaturation) as expressed by the factor R in eqn [5]. The effective R at which sulfide is formed is shown in **Figure 8(b)** for each of the three scenarios, again as a function of the temperature during the assimilation–crystallization process.

Figure 8(c) shows the compositions of the sulfide liquids that would result from the different extents of assimilation and crystallization modeled in **Figure 8(a)** and **8(b)**. In all three cases, at the point at which sulfide is barely supersaturated, the quantity of sulfide present is very small, so R is very large. In these cases, the PGE concentration in the sulfide is extremely high, and the base metal content approaches the limiting value of C_oD. When the system has crystallized more cumulates and more sulfide has been precipitated, the three scenarios show very different results. The sulfide-rich assimilant causes the generation of a much larger quantity of sulfide melt that has much lower PGE concentrations and somewhat lower copper concentrations than are seen in the case of the assimilation of sulfur-free semipelite or no assimilation at all. This is a direct consequence of the fact that if a larger quantity of sulfide melt is equilibrated with a given quantity of silicate melt, effectively all of the PGE in the bulk system will reside in the sulfide in both cases, but if there is more sulfide melt, the PGE will simply be diluted.

The practical consequences of the behavior shown in **Figure 8** are that a magma allowed to cool and crystallize in relative isolation can eventually become saturated with small quantities of sulfide melt with very high PGE tenor. The same parental magma, if it assimilates S-poor crustal rocks, may become saturated somewhat later with a similarly high-tenor sulfide. The timing of sulfide saturation is extremely sensitive to the sulfur content of the assimilant. If, instead, the magma encounters S-rich metasedimentary rocks, it will precipitate a much greater mass of relatively PGE-poor sulfide melt early in its history. Because the partition coefficients of base metals are smaller than those of the precious metals, the dependence of the concentrations of copper, nickel, and cobalt on the degree of sulfide supersaturation (i.e., smaller R) is less pronounced. The assimilation of sulfur-rich sediments is therefore a suitable pathway to the formation of large quantities of sulfide liquid rich in base metals, such as copper, nickel, and cobalt, but relatively poor in PGE, whereas the formation of a PGE-rich sulfide melt is more likely to result from sulfide saturation without addition of external sulfur.

Early saturation with sulfide, before significant amounts of olivine have been removed by fractional crystallization, will result in the segregation of Ni-rich sulfide, with a high Ni/Cu ratio. If sulfide saturation occurs after extensive olivine fractionation, it will have a much lower Ni/Cu ratio. Furthermore, magmas derived by moderate amounts of partial melting have lower Ni/Cu than those produced by very large degrees of melting (**Figure 4**). For these reasons, magmatic sulfides associated with ultramafic magmas tend to have a much higher Ni/Cu ratio than those hosted by basaltic magmas.

Silicate melts that have reacted with sulfide melt at low R will show strong palladium depletion but will retain much of their copper, giving them a higher Cu/Pd ratio compared with primitive sulfide-undersaturated magmas. Silicate magmas that have accumulated small amounts of sulfide will similarly

show a large decrease in Cu/Pd, an observation that can be used to detect the presence of minor quantities of cumulus sulfide in layered intrusions (Maier and Barnes, 2005).

If a magma chamber is fractionating as a closed system, then the Cu/Pd ratio will rest close to values representative of the parental magma in early formed cumulates and their residual liquids because both elements are incompatible in rock-forming silicate magmas. When the magma reaches sulfide saturation, the first sulfides deposited will contain most of the palladium in the entire magma chamber, causing a sudden spike to very low values of Cu/Pd in the whole rock at the stratigraphic level of the reef. Once the palladium has been sequestered into the early formed sulfide melt, any subsequent cumulus silicates and sulfides will show much higher Cu/Pd than the initial ratio. The spatial variation of the ratio therefore can be, and has been, used successfully to locate cryptic or unexposed sulfide accumulation horizons of possible economic significance in layered intrusions (Maier and Barnes, 2005; Nielsen et al., 2005) and to detect a signature reflecting removal of ore-forming sulfides from basalts prior to their eruption (Lightfoot and Keays, 2005).

To illustrate the importance of PGE depletion signatures in the recognition that a magma has generated potentially valuable sulfides, **Figure 8(d)** and **8(e)** shows the compositions of basaltic liquids from which sulfide liquids have been extracted in the models shown in **Figure 10(a)–10(c)**, compared with the compositions of basalts from the Siberian traps. The basalts of the Nadezhdinsky formation are evidently very strongly depleted in chalcophile elements and highly enriched in zirconium. These compositions can be interpreted to result from assimilation of Zr-rich sediment followed by equilibration with a sulfide melt at a relatively low silicate/sulfide ratio. A few samples of the Morongovsky formation show a relatively subtle signature of mild palladium depletion that may record equilibration with a sulfide liquid at a very high silicate/sulfide ratio. The other lavas of the suite show evidence neither for assimilation of sediment nor for equilibration with sulfide liquid, implying that they did not leave sulfide ores behind them in the crustal conduit systems that fed them. The detailed interpretation of these and similar signatures remains a topic of heated debate in the recent literature, but there is a consensus that it is the subtle depletion signature in the Morongovsky formation basalts that points to high grade magmatic sulfides of the Noril'sk–Talnakh camp.

Significant changes in sulfide melt composition may occur in a magma conduit because of the reaction of early formed sulfide melt with fresh, sulfide-undersaturated, and PGE-undepleted magma due to either settling of sulfide droplets through a magma column or continuous reaction with undepleted magma as it passes by the site of deposition of the sulfide melt. The consequences of this process were thoroughly explored by Kerr and Leitch (2005), who showed that dissolution of preexisting sulfide by new pulses of sulfide-undersaturated and PGE-undepleted magma can lead to extreme increases in metal tenor while substantially diminishing the total amount of sulfide melt present. An important consequence of these effects is that if sulfide has been redissolved, any attempt to apply eqn [5] to infer the characteristics of an inferred hidden ore deposit based on measured rock compositions could lead to misleading results.

13.8.6.5 Crystallization of Sulfide Magmas

If sulfide segregation takes place at a relatively small R value (e.g., R = several hundred at Sudbury; Naldrett et al., 1999) or if higher R-value sulfide melt is able to accumulate efficiently from an extremely large volume of magma (e.g., R = several thousand at Noril'sk; Lightfoot and Keays, 2005), a pool of sulfide melt can form wherever a hydrodynamic trap exists in which it can collect. Typical natural sulfide magmas have compositions in the range 0–10% nickel, 0–35% copper, 32–36% sulfur, and 0–4% oxygen, with the remainder being iron. A classic example of a large differentiated magmatic sulfide system is the collection of orebodies around the base of the Sudbury Igneous Complex (SIC). At Sudbury, disseminated sulfides hosted by noritic cumulate rocks overlie local accumulations of Ni- and IPGE-rich massive sulfides that occupy the basal contact of the SIC. The sulfides are interpreted to have settled out of a sulfide-saturated magma that was generated as a meteorite impact melt sheet (e.g., Grieve et al., 1991; Keays and Lightfoot, 2004; Li and Ripley, 2009). Below the basal contact, veins composed of copper-, platinum- palladium-, and gold-rich massive sulfide with variable nickel content occur, locally flanked by halos of disseminated copper and nickel sulfides with extraordinarily high contents of platinum, palladium, and gold (e.g., Farrow et al., 2005; Naldrett et al., 1999).

When they form by liquation from basaltic magmas at temperatures between 1400 and 1200 °C, sulfide melts are far above their liquidus temperatures. As they cool, sulfide melts begin to crystallize either mss or magnetite at temperatures between 1000 and 1200 °C (Ballhaus et al., 2001; Ebel and Naldrett, 1996, 1997; Fleet and Pan, 1994; Fleet et al., 1993; Li et al., 1996; Mungall, 2007; Mungall et al., 2005; Naldrett, 1969; Naldrett et al., 1997). The eutectic in the Fe–S–O system is at 915 °C (Naldrett, 1969), but the addition of copper and nickel can depress the temperature of final crystallization to well below 800 °C (Craig and Kullerud, 1969). The possible presence of highly incompatible minor elements such as Ag, As, Sb, Te, (Frost et al., 2002), Cl (Mungall and Brenan, 2003), and possibly H_2O (Wykes and Mavrogenes, 2005) might permit sulfide melts to persist to temperatures below 700 °C in exceptional cases.

A number of workers have demonstrated that the variations in composition of sulfide ores at Noril'sk (Naldrett et al., 1997) and Sudbury (Li and Naldrett, 1994; Naldrett et al., 1999) are best accounted for by models of mss fractionation, possibly followed at low temperatures by fractionation of intermediate solid solution, a phase with a composition similar to that of chalcopyrite.

Empirical parameterizations of the partition coefficients of the chalcophile elements between mss and sulfide melt are presented in **Table 3** (Mungall, 2007). In high temperature Fe–Ni–Cu–S–O magmas, the IPGE are strongly compatible with mss, having partition coefficients of on the order of 10, whereas platinum, palladium, and gold are highly incompatible with mss and are always concentrated in residual sulfide melt during mss fractionation. At high temperatures, the mss contains less nickel and copper than the sulfide melt, but as temperature falls, D_{Ni} rises to approach 1, and at the lowest temperatures at which natural sulfide magmas exist, nickel is compatible in mss (Barnes and Maier, 1999; Mungall, 2007;

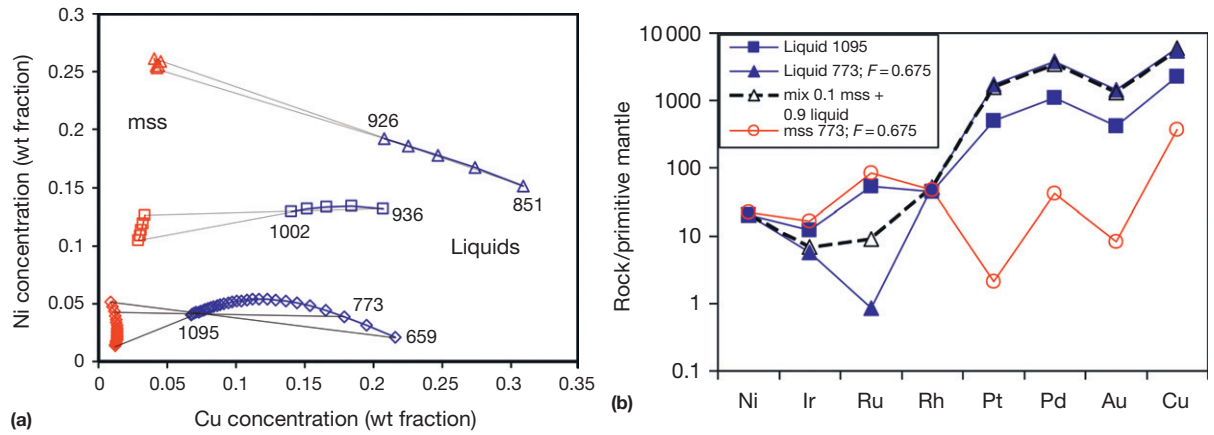

Figure 9 Compositional variation in sulfide magmas during monosulfide solid solution (mss) crystallization. (a) Ni versus Cu (wt%) in model liquids (curves at right) and mss (curves at left). Selected coexisting mss and liquid compositions are joined by tie-lines. Note that tie-lines pivot around initial liquid compositions because this diagram shows products of equilibrium crystallization. The two metal-rich trends beginning with melt compositions near 0.1 and 0.15 Ni were calculated for O-free systems. The trend from 1095 to 659 °C is typical of natural sulfide magmas formed with initial Cu and Ni contents near 5 wt% and O content of about 2 mol%. Note that Ni does not become compatible with mss until temperatures have dropped below 800 °C in metal-poor systems such as this. (b) Element ratio plot showing PGE concentrations in sulfide melt and mss, normalized to primitive mantle (McDonough and Sun, 1995). The initial liquid at 1095 °C (squares) is based on a typical massive sulfide sample from the Mesamax deposit, northern Quebec (Mungall, unpublished data). When 67.5% of the magma has solidified, mss (circles) has low Pt, Pd, Au, and Cu but high Ni, Ir, and Ru concentrations relative to the residual melt (triangles). The dashed line shows a mixture comprising 10% mss and 90% liquid, such as might be found in a vein of fractionated sulfide crystallized at some distance from the site of the main sulfide body.

Mungall et al., 2005). These relations are shown in **Figure 9(a)**, which illustrates nickel and copper concentrations in sulfide melt and mss cumulates calculated using relations in **Table 3**. Liquidus temperatures of the initial and final liquids produced by equilibrium crystallization of three different starting compositions are indicated on the diagram. The concentration of nickel in mss does not exceed that in the residual sulfide melt at temperatures above 800 °C unless the initial melt composition is very rich in nickel and copper. The behavior of the PGE in sulfide magmas is illustrated in **Figure 9(b)**, an element ratio plot showing the compositions of the initial liquid and final liquids at the bottom of **Figure 9(a)**. The model results shown for the lowest three temperatures (773–659 °C) in the run with the lowest metal contents are below the solidus temperature of the Fe–Ni–Cu–S system and are therefore speculative extrapolations based on the hypothetical effects of fluxing agents such as Cl, O, or H_2O. After cooling to 773 °C, the system crystallizes to a weight fraction of 0.675 mss cumulates (circles), which are slightly enriched in nickel, rhodium, and ruthenium relative to the melt but are strongly depleted in platinum, palladium, gold, and copper, whereas the 0.325 residual melt is enriched in platinum, palladium, gold, and copper.

In light of the observation that massive sulfide ores interpreted as mss cumulates are usually enriched in both nickel and IPGE, it has been suggested that in many situations, the process of sulfide crystallization tends to take place at equilibrium in closed systems until the enclosing silicate rocks are completely solidified (Mungall et al., 2005). Once the host rocks are brittle solids, the small amounts of sulfide melt that remain are able to migrate away from the cumulates to form veins and disseminations of Cu-rich sulfide (Mungall and Su, 2005). As the late sulfide migration may take place at different temperatures in different systems, there is a wide range of possible nickel contents for magmatic sulfide vein deposits, depending on the particular value of D_{Ni} at which the mss and liquid became separated. For example, at Noril'sk, the sulfide ores show a pattern of initial Ni enrichment during fractionation, followed by Ni depletion – this can be interpreted as resulting from relatively early separation of Ni-poor mss from Ni-rich residual sulfide melt at a relatively high temperature in a process more nearly approximating fractional crystallization (Naldrett et al., 1997). Migration of sulfide liquid away from mss cumulates late in the cooling of a magmatic system occurs not only in massive sulfide bodies but also over distances of hundreds of meters in disseminated or blebby sulfides within the norites overlying the main massive sulfide orebodies, as has been inferred to have occurred at Sudbury (Mungall, 2002b).

The low-sulfide PGE deposits that form as disseminated halos around the fractionated Cu-rich vein deposits at Sudbury may represent the last, most fractionated sulfide liquids in the system, or they might have formed because of the release of PGE-rich aqueous fluids, carbonic fluids, or halide melts from crystallizing magmatic sulfide veins (Hanley et al., 2005a).

13.8.6.6 Precious Metal Sulfide Deposits

13.8.6.6.1 Classification

When sulfide liquid equilibrates with silicate melt at very high R values, the resulting composition can be sufficiently enriched in PGE to form economic deposits at sulfide modal abundances well below 10%. In these cases, the principal value contained in the deposit comes from the PGE rather than the copper and nickel. Although there are examples of PGE sulfide deposits in irregularly shaped magmatic intrusions

perhaps best described as conduits (e.g., Lac Des Iles; Hinchey et al., 2005) or as basal accumulations around the margins of mafic intrusions (e.g., the Platreef of the northern Bushveld intrusion; Kinnaird et al., 2005), the majority of PGE sulfide deposits are situated in stratiform bodies commonly referred to as reefs, within mafic or ultramafic layered intrusions.

Stratiform PGE occurrences can be classified into two principal groups: the offset and unconformity types. Offset PGE reefs are so called because the individual PGE are enriched at different levels so that the highest grade accumulations of the metals are offset from each other stratigraphically within layers that are conformable with the layering of the silicate cumulate rocks. The unconformity type is contained in minor sulfide accumulations associated with magmatic unconformities of regional extent in the Stillwater and Bushveld intrusions. Each of these types is discussed, in turn.

13.8.6.6.2 Offset reefs

As sulfide liquid first begins to precipitate in a previously sulfide-undersaturated magma in a large layered intrusion, it will do so initially at an extremely large R value. The earliest formed sulfide droplets will contain the PGE with the highest partition coefficients in preference to other elements with slightly lower partition coefficients. The earliest formed layer of accumulated sulfide will therefore be highly enriched in PGE relative to copper and nickel. Continued slow extraction and accumulation of very small amounts of sulfide from the magma will take place from a progressively more PGE-depleted silicate melt, leading to gradual drops in PGE concentration in the accumulated sulfide. Once the modal abundance of sulfide in the cumulate reaches its cotectic proportion (close to its solubility of about 1000 ppm sulfur, or 2750 ppm FeS), the PGE will have already been depleted from the silicate melt, but gold and, later, copper, will remain high enough to enter the sulfide melt in considerable amounts. The resulting reef deposit will contain a peak palladium and platinum concentration some distance below a gold peak, with maximum copper concentrations occurring somewhere above both. This concept was first proposed by Naldrett and Wilson (1990). Barnes (1993) was unable to reproduce exactly the pattern of distribution of base and precious metals in offset mineralization in the Munni Munni intrusion of Australia and found that the partition coefficients for the PGE needed to be manipulated in an ad hoc manner; he then proposed that other phases such as alloy might be controlling PGE distribution in the reef.

A solution to the problems with the partition coefficients was proposed by Mungall (2002c), who showed that when sulfide first appears in the magma chamber, it is likely to do so under conditions of moderate supersaturation, because of kinetic constraints on droplet nucleation (Mungall and Su, 2005). The few widely spaced droplets that result from inhibited nucleation will be able to grow and settle from a silicate melt that remains supersaturated throughout the career of each drop. In this case, partitioning is driven not so much by the equilibrium partition coefficient as by the diffusivity of the metals through the silicate melt and by the degree of supersaturation. Using models that take these parameters into account, Mungall (2002c) demonstrated that the pattern of base and precious metal distribution at Munni Munni could be interpreted in a fully self-consistent model that used the concentration of copper to predict the concentrations of all other elements without any adjustable parameters (**Figure 10**).

Offset PGE reefs can thus be considered to result from the fractional segregation and accumulation of sulfide droplets from a basaltic melt that is mildly supersaturated with respect to sulfide melt.

An opposing view is that the offsets in PGE and base metal distribution arise from the chromatographic separation of chalcophile elements as they are transported upward by deuteric fluids streaming out of the cumulate pile as it cools and reaches vapor saturation (Boudreau and McCallum, 1992; Boudreau and Meurer, 1999). This concept, which is further described in the following sections, can produce model stratigraphic element distribution profiles such as those produced by the fractional sulfide accumulation model described earlier. The distinction between the two models must therefore be made on other grounds.

The resolution to the issue may lie on the length scale at which the two proposed phenomena would take place. Fluid migration is a local process, whose rate is locally determined by factors such as porosity, melt viscosity, and cumulate layer thickness, all of which are indirectly functions of temperature and cooling rate and are expected to vary from place to place within the cumulate pile. It should therefore be expected that fluid migration fronts will not follow the original stratigraphic horizons faithfully. Any local phenomenon such as opening of pore space by remelting of cumulates in the presence of augmented volatile concentrations would also tend to break a migrating fluid front into slower-moving fronts and faster-moving nodes into which the fluids could then drain laterally. On the other hand, disturbances in a magma chamber will tend to spread laterally so as to eliminate lateral variations in buoyancy. Sulfide saturation would therefore be expected to occur simultaneously throughout a magma chamber, leading to the deposition of sulfide at the same point in the cumulus stratigraphy everywhere. Large-scale lateral differences in cumulate thickness would not interfere with the simultaneous deposition of the sulfides at the equivalent place in the cumulate pile. For these reasons, the magmatic hypothesis for the generation of offset PGE reefs is compelling; however, as discussed in the following sections, the idea of fluid transfer of PGE in cumulates is important and may dominate PGE deposition in some other environments.

13.8.6.6.3 Unconformity-hosted reefs

The Merensky Reef, UG1, and UG2 chromitite horizons of the Bushveld complex (Cawthorn, 2005a,b; Cawthorn et al., 2002) and the J-M Reef of the Stillwater intrusion (Zientek et al., 2002) together account for a major portion of the world's known resources of platinum and palladium. A successful model for the petrogenesis of these deposits must be able to account for a unique series of geological attributes that are shared by these deposits.

The definitive characteristic of unconformity-type reef deposits is the presence of a PGE-enriched stratum directly overlying a regionally extensive magmatic unconformity. Rocks of the reef package form a recognizable stratigraphic unit that drapes a highly irregular surface, truncating layering in earlier cumulate rocks. In the UG1, UG2, and

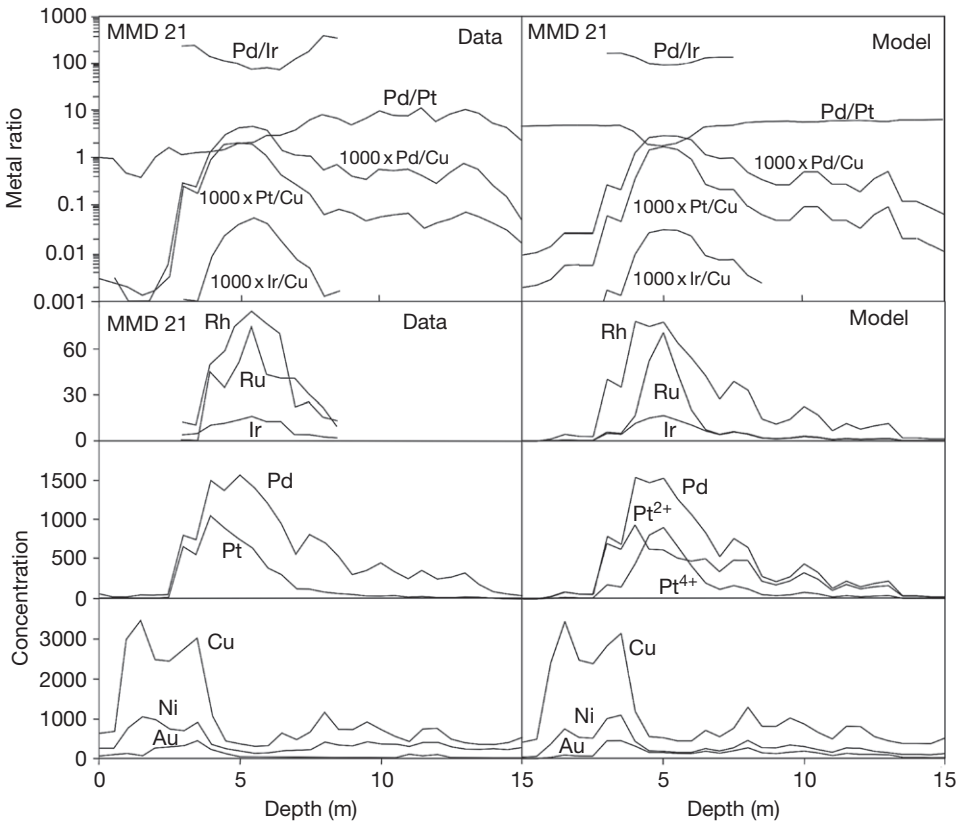

Figure 10 Formation of offset reefs by fractional segregation of sulfide melt. The curves on the left are assay data from a borehole through an offset reef hosted by websterite cumulates in the Munni Munni intrusion of Australia (Barnes, 1993). The curves on the right are model element concentrations and ratios calculated according to the kinetically controlled sulfide segregation model of Mungall (2002c), using the concentration of Cu in the assay data to estimate the modal abundance of sulfide and hence the degree of sulfide supersaturation. Reproduced with permission from Mungall JE (2002) Kinetic controls on the partitioning of trace elements between silicate and sulfide liquids. Journal of Petrology 43: 749–768.

Merensky Reefs, this topography is dominated by locally or regionally developed depressions known as potholes (e.g., Cawthorn et al., 2002; Leeb-Du Toit, 1986; Viljoen and Hieber, 1986); the J-M Reef overlies a surface that cuts down through several hundred meters of older mafic cumulates, being locally present directly on the basal ultramafic series, and shows local thickened portions, known as ballrooms, that transgress the underlying stratigraphy (Boudreau, 1992, 1999a; Turner et al., 1985).

A secondary characteristic of unconformity-type reefs within the Bushveld intrusion is a radical upward increase in the abundance of radiogenic strontium and osmium at the level of the reef (Kruger, 1994; Schoenberg et al., 1999). The increase in abundance of radiogenic osmium is confined to the Merensky reef itself, whereas the increased $^{87}Sr/^{86}Sr$ signature persists through several thousand meters of overlying cumulates.

A tertiary feature of unconformity-type PGE reefs is that they mark the stratigraphic level of a marked change in the compositions of hydrous cumulus and postcumulus igneous minerals such as apatite and biotite, from Cl-rich compositions, reflecting equilibration with an aqueous fluid below the reef, to F-rich compositions, reflecting equilibration with Cl-poor silicate melt above the reef (Boudreau et al., 1986; Willmore et al., 2000).

The cumulate sequence underlying the UG1, UG2, and Merensky Reef horizons of the Bushveld intrusion contains significant concentrations of intercumulus sulfide and has variable platinum concentrations of approximately 25–75 ppb throughout its height (Maier and Barnes, 1999). This, and its generally ultramafic character, can be used as evidence that the early history of crystal accumulation in the Bushveld intrusion involved sedimentation of crystals and immiscible sulfide liquid in almost cotectic proportions from a system open to inputs of fresh magma that was, or became, sulfide saturated and outputs of fractionated, PGE-depleted silicate magma (Barnes and Maier, 2002). The deficit of sulfur relative to cotectic proportions may result from the crystallization of a portion of each new pulse of magma before reaching sulfide saturation or from the subsequent removal of some sulfur in aqueous fluids.

Two principal hypotheses have been advanced to explain the petrogenesis of unconformity-type PGE reefs. The main points of each group are briefly reviewed without engaging in a detailed critique of either.

One group has argued that unconformity-type PGE reefs form as a result of sulfide liquid immiscibility provoked by a magma recharge and mixing events (e.g., Campbell et al., 1983; Irvine, 1977; Irvine et al., 1983; Kruger, 2005; Maier and Barnes, 1999; but see also Cawthorn, 2002; Naldrett

et al., 2009a,b). This hypothesis requires that the hybrid magma was sulfide-oversaturated, with a very large silicate/sulfide mass ratio, but that prior and subsequent magma recharge events failed to achieve sulfide saturation at the critical *R*-factor required to generate an economic sulfide concentration. The change in crystallization sequence and isotope geochemistry at the level of the reef is accounted for as a consequence of the introduction to the system of magma of an entirely different lineage. The unconformity and pothole development are thought to result from local thermal erosion.

The other group points out that silicate magmas always contain some small amount of dissolved H_2O and that this will inevitably be released to form a deuteric aqueous fluid upon complete crystallization of whatever silicate melt is trapped between cumulus phases in a growing cumulate pile (e.g., Ballhaus and Stumpfl, 1986; Boudreau, 1992, 1999a; Boudreau and McCallum, 1992; Boudreau and Meurer, 1999; Mathez et al., 1989). Whereas intercumulus melt at the site of the release of deuteric fluids is obviously vapor-saturated, the overlying partially molten cumulus pile is not. Deuteric fluids will therefore be isolated from the main magma chamber by a vapor-undersaturated zone in the upper reaches of the cumulate pile and will evolve independently of the magma and the newly forming cumulates (**Figure 11**). As S-rich deuteric fluids rise to the top of the vapor-saturated zone and encounter vapor-undersaturated intercumulus silicate melt, they redissolve. Such fluids may carry significant concentrations of the PGE (Hanley et al., 2005b, 2008; Simon and Pettke, 2009). Since the solubility of sulfide in silicate melt is about 1000 ppm, whereas its solubility in the aqueous fluid may exceed several weight percent, both the excess sulfide and any PGE that may have been scavenged by the deuteric fluid will be deposited at the rising vapor-saturation front. The result is that PGE are stripped from the vapor-saturated zone and redeposited in the upward-migrating vapor-saturation front to form a regionally extensive PGE-rich sulfide zone that is epigenetic and discordant with respect to the primary igneous stratigraphy. Localization of this intrinsically discordant feature within concordant stratigraphic horizons in the cumulate sequence is the most notable target for criticisms of the deuteric model; defenders of the model argue for the stranding of upward-migrating sulfide-saturation zones within layers having unusually high primary cumulate porosity or under layers through which fluids are unable to migrate for structural reasons.

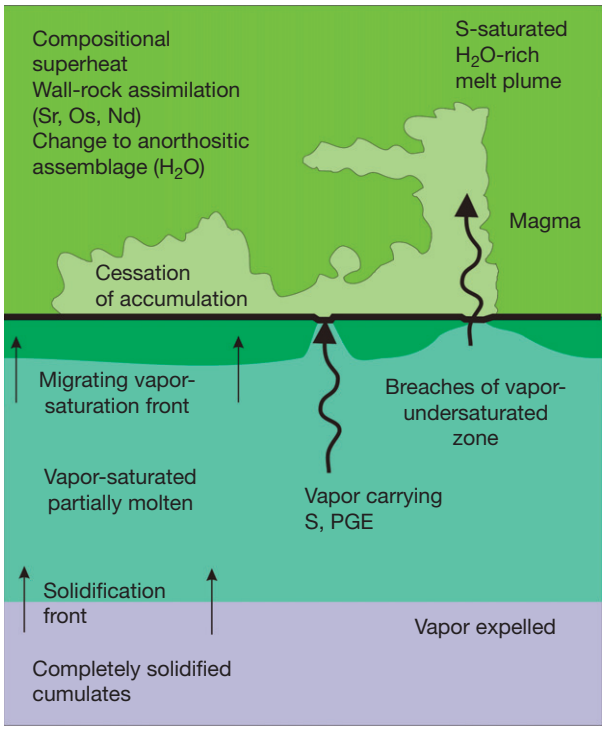

Figure 11 Cartoon of a layered intrusion illustrating the formation of an unconformity-type PGE reef (heavy black line) due to the venting of S-saturated aqueous fluids from the cumulate pile into a magma chamber.

Without detailing the many arguments that have been raised against both of these hypotheses, the continuing vigor of the debate after more than 20 years of research indicates that neither has successfully accounted for all the geological observations of the structure, petrology, and geochemistry of unconformity-type stratiform PGE reefs. It is striking that elaborate forward models of the geochemistry of the systems in question are successful at replicating the observed vertical distribution of rock types and PGE mineralization in both the orthomagmatic models (e.g., Naldrett et al., 2009a,b) and the hydromagmatic models (e.g., Boudreau and McCallum, 1992) despite the obvious fact that at any one time and place, only one of the two hypotheses can be correct.

In summary, there are several competing concepts for the genesis of stratiform precious metal deposits in layered intrusions, and indeed, there is probably a different model for each geologist. Each deposit undoubtedly formed in an environment different from all others, and there is therefore no single ore deposit model that can account for all the observations. The key factors are undoubtedly the combination of the very high compatibility of the PGE and gold in sulfide melt, and the need for a source–transport–trap process to operate simultaneously through vast volumes of magma and/or cumulate rocks.

13.8.7 Conclusions

The discussion of processes leading to the generation of magmatic ores leads one through a tremendous range of magma types and tectonic or structural settings. Most of the situations in which these deposits form represent unusual convergences of factors, so the magmas involved are atypical. The vast majority of magmatic activity on Earth is represented by MORB, OIB, and common arc tholeiitic to calc-alkaline magmas, all of which are conspicuously bereft of ore deposits. It is the rare and unusual processes, producing boninites, carbonatites, komatiites, sulfide magmas, Fe oxide magmas, or water-undersaturated felsic rare-element granites, that produce ore deposits. For this reason, the precepts that govern conventional igneous petrology, such as the immensely successful theory of crystallization differentiation, have to make room for less familiar but fascinating concepts, such as liquid immiscibility or fluid fluxing of cumulates, in the search for explanations of the tremendously valuable geochemical anomalies called ore deposits.

Acknowledgments

The ideas expressed in this chapter are distilled from readings and discussions with many colleagues over several years, notably Tony Naldrett, Nick Arndt, Wolf Maier, Sarah Jane Barnes, Steve Barnes, and Alan Boudreau.

References

Alapieti TT, Kujanpaa J, Lahtinen JJ, and Papunen H (1989) The Kemi stratiform chromitite deposit, northern Finland. *Economic Geology* 84: 1057–1077.

Arai S and Matsukage K (1998) Petrology of chromitite micropod from Hess Deep, equatorial Pacific: A comparison between abyssal and Alpine-type podiform chromitites. *Lithos* 43: 1–14.

Arndt NT, Czamanske GK, Walker RJ, Chauvel C, and Fedorenko VA (2003) Geochemistry and origin of the intrusive hosts of the Noril'sk-Talnakh Cu-Ni-PGE sulfide deposits. *Economic Geology* 98: 495–513.

Augé T, Genna A, Legendre O, Ivanov KS, and Volchenko YA (2005) Primary platinum mineralization in the Nizhny Tagil and Kachkanar ultramafic complexes, Urals, Russia: A genetic model for PGE concentration in chromite-rich zones. *Economic Geology* 100: 707–732.

Ballhaus C and Stumpfl EF (1986) Sulfide and platinum mineralization in the Merensky Reef: Evidence from hydrous silicates and fluid inclusions. *Contributions to Mineralogy and Petrology* 94: 193–204.

Ballhaus C, Tredoux M, and Späth A (2001) Phase relations in the Fe–Ni–Cu–PGE–S system at magmatic temperature and application to massive sulphide ores of the Sudbury Igneous Complex. *Journal of Petrology* 42: 1911–1926.

Barnes SJ (1993) Partitioning of the platinum-group elements and gold between silicate and sulfide magmas in the Munni Munni Complex, Western Australia. *Geochimica et Cosmochimica Acta* 57: 1277–1290.

Barnes SJ (1998) Chromite in komatiites, 1. Magmatic controls on crystallization and composition. *Journal of Petrology* 39: 1689–1720.

Barnes SJ and Fiorentini ML (2008) Iridium, ruthenium and rhodium in komatiites: Evidence for iridium alloy saturation. *Chemical Geology* 257: 44–58.

Barnes S-J and Maier W (1999) The fractionation of Ni, Cu and the noble metals in silicate and sulphide liquids. In: Keays RR, Lesher CM, Lightfoot PC, and Farrow CEG (eds.) *Dynamic Processes in Magmatic Ore Deposits and their Application to Mineral Exploration, Geological Association of Canada Short Course Notes*, vol. 13, pp. 69–106. St. John's, NL: Geological Association of Canada.

Barnes S-J and Maier W (2002) Platinum-group element distributions in the Rustenburg Layered Suite of the Bushveld Complex, South Africa. In: Cabri LJ (ed.) *The Geology, Geochemistry, Mineralogy and Mineral Beneficiation of Platinum-Group Elements*, CIM Special Volume 54, pp. 431–458. Montreal: Canadian Institute of Mining, Metallurgy and Petroleum.

Bézos A, Lorand J-P, Hummler E, and Gros M (2005) Platinum-group element systematics in mid-ocean ridge basaltic glasses from the Pacific, Atlantic and Indian oceans. *Geochimica et Cosmochimica Acta* 69: 2613–2627.

Blundy J and Wood B (2003) Partitioning of trace elements between crystals and melts. *Earth and Planetary Science Letters* 210: 383–397.

Bockrath C, Ballhaus C, and Holzheid A (2004) Fractionation of the platinum-group elements during mantle melting. *Science* 304: 1951–1953.

Boettcher AL and Wyllie PJ (1969) Phase relationships in system $NaAlSiO_4$-SiO_2-H_2O to 35 kilobars pressure. *American Journal of Science* 267: 875–909.

Borisov A and Palme H (2000) Solubilities of noble metals in Fe-containing silicate melts as derived from experiments in Fe-free systems. *American Mineralogist* 85: 1665–1673.

Boudreau AE (1992) Volatile fluid overpressure in layered intrusions and the formation of potholes. *Australian Journal of Earth Sciences* 39: 277–287.

Boudreau AE (1999a) Fluid fluxing of cumulates: The J-M reef and associated rocks of the Stillwater complex, Montana. *Journal of Petrology* 40: 755–772.

Boudreau AE (1999b) PELE – A version of the MELTS software program for the PC platform. *Computers and Geosciences* 25: 201–203.

Boudreau AE, Mathez EA, and MacCallum IS (1986) Halogen geochemistry of the Stillwater and Bushveld complexes: Evidence for transport of the platinum-group elements by Cl-rich fluids. *Journal of Petrology* 27: 967–986.

Boudreau AE and McCallum IS (1992) Concentration of platinum-group elements by magmatic fluids in layered intrusions. *Economic Geology* 87: 1830–1848.

Boudreau AE and Meurer WP (1999) Chromatographic separation of the platinum-group elements, gold, base metals and sulfur during degassing of a compacting and solidifying igneous crystal pile. *Contributions to Mineralogy and Petrology* 134: 174–185.

Brenan JM (2002) Re–Os fractionation in magmatic sulfide melt by monosulfide solid solution. *Earth and Planetary Science Letters* 199: 257–268.

Brenan JM (2008) Re–Os fractionation by sulfide melt–silicate melt partitioning: A new spin. *Chemical Geology* 248: 140–165.

Brenan JM, McDonough WF, and Ash R (2005) An experimental study of the solubility and partitioning of iridium, osmium and gold between olivine and silicate melt. *Earth and Planetary Science Letters* 237: 855–872.

Brenan JM, McDonough WF, and Dalpe C (2003) Experimental constraints on the partitioning of rhenium and platinum-group elements between olivine and silicate melt. *Earth and Planetary Science Letters* 212: 135–150.

Broman C, Nystrom JO, Henriquez F, and Elfman M (1999) Fluid inclusions in apatite from a cooling magmatic system at El Laco, Chile. *GFF* 121: 253–267.

Brugmann GE, Naldrett AJ, Asif M, Lightfoot PC, Gorbachev NS, and Fedorenko VA (1993) Siderophile and chalcophile metals as tracers of the evolution of the Siberian trap in the Norilsk region, Russia. *Geochimica et Cosmochimica Acta* 57: 2001–2018.

Buhn B and Rankin AH (1999) Composition of natural, volatile-rich Na–Ca–REE–Sr carbonatitic fluids trapped in fluid inclusions. *Geochimica et Cosmochimica Acta* 63: 3781–3797.

Campbell IH and Naldrett AJ (1979) The influence of silicate:sulfide ratios on the geochemistry of magmatic sulfides. *Economic Geology* 74: 1503–1505.

Campbell IH, Naldrett AJ, and Barnes SJ (1983) A model for the origin of the platinum-rich sulfide horizons in the Bushveld and Stillwater complexes. *Journal of Petrology* 24: 133–165.

Cawthorn RG (2002) The role of magma mixing in the genesis of PGE mineralization in the Bushveld complex: Thermodynamic calculations and new interpretations – A discussion. *Economic Geology* 97: 663–667.

Cawthorn RG (2005a) Stratiform PGE deposits in layered intrusions. In: Mungall JE (ed.) *Exploration for Deposits of Platinum-Group Elements, Mineralogical Association of Canada Short Course Series*, vol. 35, pp. 57–73. Quebec: Mineralogical Association of Canada.

Cawthorn RG (2005b) Pressure fluctuations and the formation of the PGE-rich merensky and chromitite reefs, Bushveld complex. *Mineralium Deposita* 40: 231–235.

Cawthorn RG, Merkle RKW, and Viljoen MJ (2002) Platinum-group element deposits in the Bushveld complex, South Africa. In: Cabri LJ (ed.) *The Geology, Geochemistry, Mineralogy and Mineral Beneficiation of Platinum-Group Elements*, CIM Special Volume 54, pp. 389–429. Montreal: Canadian Institute of Mining, Metallurgy and petroleum.

Cerny P (1992) Geochemical and petrogenetic features of mineralization in rare-element granitic pegmatites in the light of current research. *Applied Geochemistry* 7: 393–416.

Clark AH and Kontak DJ (2004) Fe–Ti–P oxide melts generated through magma mixing in the Antauta subvolcanic center, Peru: Implications for the origin of nelsonite and iron oxide-dominated hydrothermal deposits. *Economic Geology* 99: 377–395.

Craig JR and Kullerud G (1969) Phase relations in the Fe–Ni–Cu–S system and their application to magmatic ore deposits. *Economic Geology Monograph* 4: 344–358.

Crocket JH (2002) Platinum group element geochemistry of mafic and ultramafic rocks. In: Cabri LJ (ed.) *The Geology, Geochemistry, Mineralogy and Mineral Beneficiation of Platinum-Group Elements*, CIM Special Volume 54, pp. 177–210. Montreal: Canadian Institute of Mining, Metallurgy and Petroleum.

Czamanske GK, Zen'ko TE, Fedorenko VA, et al. (1995) Petrographic and geochemical characterization of ore-bearing intrusions of the Noril'sk type, Siberia; with discussion of their origin. *Resource Geology Special Issue* 18: 1–48.

Dale CW, MacPherson CG, Pearson GD, Hammond SJ, and Arculus RJ (2012) Inter-element fractionation of highly siderophile elements in the Tonga Arc due to flux melting of a depleted source. *Geochimica et Cosmochimica Acta* 89: 202–225.

Ebel DS and Naldrett AJ (1996) Fractional crystallization of sulfide ore liquids at high temperature. *Economic Geology* 91: 607–621.

Ebel DS and Naldrett AJ (1997) Crystallization of sulfide liquids and the interpretation of ore composition. *Canadian Journal of Earth Sciences* 34: 352–365.

Farrow CEG, Everest JO, King DM, and Jolette C (2005) Sudbury Cu-(Ni)-PGE systems: Refining the classification using McCreedy West mine and Podolsky project case studies. In: Mungall JE (ed.) *Exploration for Deposits of Platinum-Group Elements Mineralogical Association of Canada Short Course Series*, vol. 35, pp. 163–180. Quebec: Mineralogical Association of Canada.

Fincham CJB and Richardson FD (1954) The behaviour of sulphur in silicate and aluminate melts. *Proceedings of the Royal Society Series* A-223: 40–62.

Fleet ME, Chryssoulis SL, Stone WE, and Weisener CG (1993) Partitioning of platinum-group elements and Au in the Fe–Ni–Cu–S system: Experiments on the fractional crystallization of sulfide melt. *Contributions to Mineralogy and Petrology* 115: 36–44.

Fleet ME, Crocket JH, Liu MH, and Stone WE (1999) Laboratory partitioning of platinum-group elements (PGE) and gold with application to magmatic sulfide-PGE deposits. *Lithos* 47: 127–142.

Fleet ME and Pan Y (1994) Fractional crystallization of anhydrous sulfide liquid in the system Fe–Ni–Cu–S, with application to magmatic sulfide deposits. *Geochimica et Cosmochimica Acta* 58: 3369–3377.

Force ER (1991) *Geology of Titanium-Mineral Deposits*. *Geological Society of America Special Paper*, vol. 259. Denver, CO: Geological Society of America.

Frost BR, Mavrogenes JA, and Tomkins AG (2002) Partial melting of sulfide ore deposits during medium- and high-grade metamorphism. *The Canadian Mineralogist* 40: 1–18.

Gaetani GA and Grove TL (1997) Partitioning of moderately siderophile elements among olivine, silicate melt, and sulfide melt: Constraints on core formation in the Earth and Mars. *Geochimica et Cosmochimica Acta* 61: 1829–1846.

Gao S, Luo T-C, Zhang B-R, et al. (1998) Chemical composition of the continental crust as revealed by studies in east China. *Geochimica et Cosmochimica Acta* 62: 1959–1975.

Grieve RAF, Stöffler D, and Deutsch A (1991) The Sudbury structure: Controversial or misunderstood? *Journal of Geophysical Research* 96(E5): 22753–22764.

Hammouda T (2003) High-pressure melting of carbonated eclogite and experimental constraints on carbon recycling and storage in the mantle. *Earth and Planetary Science Letters* 214: 357–368.

Hanley JJ, Mungall JE, Pettke T, Spooner ETC, and Bray CJ (2005a) Ore metal redistribution by hydrocarbon–brine and hydrocarbon–halide melt phases, North Range footwall of the Sudbury Igneous Complex, Ontario, Canada. *Mineralium Deposita* 40: 237–256.

Hanley JJ, Mungall JE, Pettke T, Spooner ETC, and Bray CJ (2008) Fluid and halide melt inclusions of magmatic origin in the ultramafic and lower banded series, Stillwater complex, Montana USA. *Journal of Petrology* 49: 1133–1160.

Hanley JJ, Pettke T, Mungall JE, and Spooner ETC (2005b) The solubility of platinum and gold in NaCl brines at 1.5 Kbar, 600 to 800°C: A laser ablation ICP-MS study of synthetic fluid inclusions. *Geochimica et Cosmochimica Acta* 69: 2593–2611.

Henriquez F and Nystrom JO (1998) Magnetite bombs at El Laco volcano, Chile. *GFF* 120: 269–271.

Herzberg C and O'Hara MJ (1998) Phase equilibrium constraints on the origin of basalts, picrites and komatiites. *Earth-Science Reviews* 44: 39–79.

Hinchey JG, Hattori KH, and Langne MJ (2005) Geology, petrology, and controls on PGE mineralization of the southern Roby and Twilight zones, Lac des Iles mine Canada. *Economic Geology* 100: 43–61.

Irvine TN (1975) Crystallization sequences in the Muskox intrusion and other layered intrusions. II. Origin of chromitite layers and similar deposits of other magmatic ores. *Geochimica et Cosmochimica Acta* 39: 991–1008.

Irvine TN (1977) Origin of chromitite layers in the Muskox intrusion and other stratiform intrusions: A new interpretation. *Geology* 5: 273–277.

Irvine TN, Keith DW, and Todd SG (1983) The J-M platinum-palladium reef of the Stillwater complex, Montana: II. Origin by double diffusive convective magma mixing and implications for the Bushveld complex. *Economic Geology* 78: 1287–1334.

Jakobsen JK, Veksler IV, Tegner C, and Brooks CK (2005) Immiscible iron- and silica-rich melts in basalt petrogenesis documented in the Skaergaard intrusion. *Geology* 33: 885–888.

Johan Z, Dunlop H, Lebel L, Robert JL, and Volfinger M (1983) Origin of chromite deposits in ophiolite complexes – Evidence for a volatile-rich and sodium-rich reducing fluid phase. *Fortschritte der Mineralogie* 61: 105–107.

Jugo PJ, Luth RW, and Richards JP (2005) Experimental data on the speciation of sulfur as a function of oxygen fugacity in basaltic melts. *Geochimica et Cosmochimica Acta* 69: 497–503.

Karabulut M, Marasinghe GK, Ray CS, et al. (2002) An investigation of the local iron environment in iron phosphate glasses having different Fe(II) concentrations. *Journal of Non-Crystalline Solids* 306: 182–192.

Katz RF, Spiegelman M, and Langmuir CH (2003) A new parameterization of hydrous mantle melting. *Geochemistry, Geophysics, Geosystems* 4: 1073.

Keays RR and Lightfoot PC (2004) Formation of Ni–Cu–platinum group element sulfide mineralization in the Sudbury impact melt sheet. *Mineralogy and Petrology* 82: 217–258.

Kerr A and Leitch AM (2005) Self-destructive sulfide segregation systems and the formation of high-grade magmatic ore deposits. *Economic Geology* 100: 311–332.

Kinnaird JA, Hutchison D, Schurmann L, Nex P, and de Lange R (2005) Petrology and mineralisation of the southern Platreef: Northern limb of the Bushveld Complex, South Africa. *Mineralium Deposita* 40: 576–597.

Kinnaird JA, Kruger FJ, and Nex PAM (2002) Chromitite formation – A key to understanding processes of platinum enrichment. *Transactions of the Institution of Mining and Metallurgy* B-111: 23–35.

Kjarsgaard BA (1998) Phase relations of a carbonated high-CaO nephelinite at 0.2 and 0.5 GPa. *Journal of Petrology* 39: 2061–2075.

Kogarko LN, Williams CT, and Woolley AR (2002) Chemical evolution and petrogenetic implications of loparite in the layered, agpaitic Lovozero complex, Kola Peninsula, Russia. *Mineralogy and Petrology* 74: 1–24.

Kolker A (1982) Mineralogy and geochemistry of Fe–Ti oxide and apatite (nelsonite) deposits and evaluation of the liquid immiscibility hypothesis. *Economic Geology* 77: 1146–1158.

Kravchenko SM, Laputina IP, Kataeva ZT, and Krasilnikova IG (1996) Geochemistry and genesis of rich Sc-REE-Y-Nb ores at the Tomtor deposit, northern Siberian platform. *Geokhimiya* 10: 938–956.

Kruger FJ (1994) The Sr-isotopic stratigraphy of the western Bushveld complex. *South African Journal of Geology* 97: 393–398.

Kruger FJ (2005) Filling the Bushveld Complex magma chamber: Lateral expansion, roof and floor interaction, magmatic unconformities, and the formation of giant chromitite, PGE and Ti-V-magnetite deposits. *Mineralium Deposita* 40: 451–472.

Laznicka P (1999) Quantitative relationships among giant deposits of metals. *Economic Geology* 94: 455–473.

Lee WJ, Fanelli MF, Cava N, and Wyllie PJ (2000) Calciocarbonatite and magnesiocarbonatite rocks and magmas represented in the system CaO-MgO-CO_2-H_2O at 0.2 GPa. *Mineralogy and Petrology* 68: 225–268.

Lee WJ and Wyllie PJ (1998) Petrogenesis of carbonatite magmas from mantle to crust, constrained by the system CaO-(MgO+FeO*)(Na_2O+K_2O)-(SiO_2+Al_2O_3+TiO_2)-CO_2. *Journal of Petrology* 39: 495–517.

Leeb-Du A (1986) The Impala Platinum Mines. In: Anhaeusser CR and Maske S (eds.) *Mineral Deposits of Southern Africa*, vol. 2, pp. 1091–1106. Johannesburg: Geological Society of South Africa.

Li C, Barnes S-J, Makovicky E, Rose-Hansen J, and Makovicky M (1996) Partitioning of Ni, Cu, Ir, Rh, Pt and Pd between monosulfide solid solution and sulfide liquid: Effects of composition and temperature. *Geochimica et Cosmochimica Acta* 60: 1231–1238.

Li C and Naldrett AJ (1994) A numerical model for the compositional variations of Sudbury sulfide ores and its application to exploration. *Economic Geology* 89: 1599–1607.

Li C and Ripley EM (2009) Sulfur contents at sulfide-liquid or anhydrite saturation in silicate melts: Empirical equations and example applications. *Economic Geology* 104: 405–412.

Li C, Ripley EM, and Naldrett AJ (2009) A new genetic model for the giant Ni-Cu-PGE sulfide deposits associated with the Siberian flood basalts. *Economic Geology* 104: 291–301.

Li C, Ripley EM, Sarkar A, Shin DB, and Maier WD (2005) Origin of phlogopite-orthopyroxene inclusions in chromites from the Merensky Reef of the Bushveld Complex, South Africa. *Contributions to Mineralogy and Petrology* 150: 119–130.

Lightfoot PC, Hawkesworth CJ, Hergt J, et al. (1993) Remobilization of continental lithosphere by mantle plumes: Major, trace element, and Sr-, Nd-, and Pb-isotopic evidence for picritic and tholeiitic basalts of the Noril'sk district, Siberian trap, Russia. *Contributions to Mineralogy and Petrology* 114: 171–188.

Lightfoot PC and Keays RR (2005) Siderophile and chalcophile metal variations in flood basalts from the Siberian trap, Noril'sk region: Implications for the origin of the Ni-Cu-PGE sulfide ores. *Economic Geology* 100: 439–462.

Lipin BR (1993) Pressure increases, the formation of chromite seams, and the development of the ultramafic series in the Stillwater complex, Montana. *Journal of Petrology* 34: 955–976.

London D (1992) The application of experimental petrology to the genesis and crystallization of granitic pegmatites. *The Canadian Mineralogist* 30: 499–540.

London D (1996) Granitic pegmatites. *Transactions of the Royal Society of Edinburgh: Earth Sciences* 87: 305–319.

London D (2008) *Pegmatites*. *Mineralogical Association of Canada Special Publication*. 10. Quebec: Mineralogical; Association of Canada.

Maier WD and Barnes S-J (1999) Platinum-group elements in silicate rocks of the lower, critical and main zones at Union Section, western Bushveld Complex. *Journal of Petrology* 40: 1641–1671.

Maier WD and Barnes S-J (2005) Lithogeochemical prospecting. In: Mungall JE (ed.) *Exploration for Deposits of Platinum-Group Elements*, *Mineralogical Association of Canada Short Course Series*, vol. 35, pp. 309–341. Quebec: Mineralogical Association of Canada.

Marquez JC and Ferreira CF (2003) The chromite deposit of the Ipueira-Medrado sill, São Francisco craton, Bahia state, Brazil. *Economic Geology* 98: 87–108.

Mathez EA, Dietrich VJ, Holloway JR, and Boudreau AE (1989) Carbon distribution in the Stillwater complex and evolution of vapor during the crystallization of Stillwater and Bushveld magmas. *Journal of Petrology* 30: 153–173.

Matveev S and Ballhaus C (2002) Role of water in the origin of podiform chromitite deposits. *Earth and Planetary Science Letters* 203: 235–243.

Mavrogenes JA and O'Neill HSC (1999) The relative effects of pressure, temperature and oxygen fugacity on the solubility of sulfide in mafic magmas. *Geochimica et Cosmochimica Acta* 63: 1173–1180.

McBirney AR and Nakamura Y (1974) Immiscibility in late-stage magmas of the Skaergaard intrusion. *Carnegie Institution of Washington Yearbook* 73: 348–352.

McDonough WF and Sun SS (1995) The composition of the Earth. *Chemical Geology* 120: 223–253.

Melcher F, Grum W, Simon G, Thalhammer TV, and Stumpfl EF (1997) Petrogenesis of the ophiolitic giant chromite deposits of Kempirsai, Kazakhstan: A study of solid and fluid inclusions in chromite. *Journal of Petrology* 38: 1419–1458.

Melcher F, Grum W, Thalhammer TV, and Thalhammer OAR (1999) The giant chromite deposits at Kempirsai, Urals: Constraints from trace element (PGE, REE) and isotope data. *Mineralium Deposita* 34: 250–272.

Mitchell RH and Kjarsgaard BA (2004) Solubility of niobium in the system $CaCO_3$-CaF_2-$NaNbO_3$ at 0.1 GPa pressure: Implications for the crystallization of pyrochlore from carbonatite magma. *Contributions to Mineralogy and Petrology* 148: 281–287.

Mondal SK and Mathez EA (2007) Origin of the UG2 chromitite layer, Bushveld Complex. *Journal of Petrology* 48: 495–510.

Mondal SK, Ripley EM, Li C, and Frei R (2006) The genesis of Archaean chromitites from the Nuasahi and Sukinda massifs in the Singhbhum Craton, India. *Precambrian Research* 148: 45–66.

Moretti R and Baker DR (2008) Modeling the interplay of fO_2 and fS_2 along the FeS-silicate melt equilibrium. *Chemical Geology* 256: 286–298.

Moretti R and Ottonello G (2005) Solubility and speciation of sulfur in silicate melts, the Conjugated Toop-Samis-Flood-Grjotheim (CTSFG) model. *Geochimica et Cosmochimica Acta* 69: 801–823.

Mungall JE (2002a) Roasting the mantle: Slab melting and the genesis of major Au and Au-rich Cu deposits. *Geology* 30: 915–918.

Mungall JE (2002b) Late-stage sulfide liquid mobility in the main mass of the Sudbury Igneous Complex: Examples from the Victor Deep, McCreedy East, and Trillabelle deposits. *Economic Geology* 97: 1563–1576.

Mungall JE (2002c) Kinetic controls on the partitioning of trace elements between silicate and sulfide liquids. *Journal of Petrology* 43: 749–768.

Mungall JE (2005) Magmatic geochemistry of the platinum-group elements. In: Mungall JE (ed.) *Exploration for Deposits of Platinum-Group Element, Mineralogical Association of Canada Short Course Series*, vol. 35, pp. 1–34. Quebec: Mineralogical Association of Canada.

Mungall JE (2007) Crystallization of magmatic sulfides: An empirical model and application to Sudbury ores. *Geochimica et Cosmochimica Acta* 71: 2809–2819.

Mungall JE, Andrews DRA, Cabri LJ, Sylvester PJ, and Tubrett M (2005) Partitioning of Cu, Ni, Au, and platinum-group elements between monosulfide solid solution and sulfide melt under controlled oxygen and sulfur fugacities. *Geochimica et Cosmochimica Acta* 69: 4349–4360.

Mungall JE and Brenan J (2003) Experimental evidence for the chalcophile behaviour of the halogens. *The Canadian Mineralogist* 41: 207–220.

Mungall JE, Hanley JJ, Arndt NT, and Debecdelievre A (2006) Evidence from meimechites and other low-degree mantle melts for redox controls on mantle-crust fractionation of platinum-group elements. *Proceedings of the National Academy of Sciences of the United States of America* 103: 12695–12700.

Mungall JE, Harvey JJ, Balch SJ, Azar B, Atkinson J, and Hamilton MA (2010) Eagle's Nest: A magmatic Ni-sulfide deposit in the James Bay Lowlands, Ontario, Canada. *Society of Economic Geologists Special Publication* 15: 539–557.

Mungall JE and Martin RF (1995) Petrogenesis of basalt-comendite and basalt-pantellerite suites, Terceira, Azores, and some implications for the origin of ocean-island rhyolites. *Contributions to Mineralogy and Petrology* 119: 43–55.

Mungall JE and Martin RF (1996) Extreme differentiation of peralkaline rhyolite, Terceira, Azores: A modern analogue for Strange Lake, Labrador? *The Canadian Mineralogist* 34: 769–777.

Mungall JE and Su S (2005) Interfacial tension between magmatic sulfide and silicate liquids: Constraints on the kinetics of sulfide liquation and sulfide migration through silicate rocks. *Earth and Planetary Science Letters* 234: 135–149.

Naldrett AJ (1969) A portion of the system Fe–S–O between 900 and 1080 °C and its application to sulfide ore magmas. *Journal of Petrology* 10: 171–201.

Naldrett AJ, Ebel DS, Asif M, Morrison G, and Moore CM (1997) Fractional crystallization of sulfide melts as illustrated at Noril'sk and Sudbury. *European Journal of Mineralogy* 9: 365–377.

Naldrett AJ, Kinnaird J, Wilson A, et al. (2009a) Chromite composition and PGE content of Bushveld chromitites: Part 1 – The lower and middle groups. *Applied Earth Science* 118: 131–161.

Naldrett AJ, Schandl E, Searcy T, Morrison GG, Binney WP, and Moore C (1999) Platinum-group elements in the Sudbury ores: Significance with respect to the origin of different ore zones and to the exploration for footwall orebodies. *Economic Geology* 94: 185–210.

Naldrett AJ and Wilson AH (1990) Horizontal and vertical zonations in noble-metal distribution in the great dyke of Zimbabwe: A model for the origin of the PGE mineralization by fractional segregation of sulfide. *Chemical Geology* 88: 279–300.

Naldrett AJ, Wilson A, Kinnaird J, and Chunnett G (2009b) PGE tenor and metal ratios within and below the Merensky Reef, Bushveld Complex: Implications for its genesis. *Journal of Petrology* 50: 625–659.

Naslund HR (1983) The effect of oxygen fugacity on liquid immiscibility in iron-bearing silicate melts. *American Journal of Science* 283: 1034–1059.

Naumov VB, Solovova IP, Kovalenker VA, and Rusinov VL (1993) Immiscibility in acidic magmas – Evidence from melt inclusions in quartz phenocrysts of ignimbrites. *European Journal of Mineralogy* 5: 937–941.

Nex PAM (2004) Formation of bifurcating chromitite layers of the UG1 in the Bushveld Igneous Complex, an analogy with sand volcanoes. *Journal of the Geological Society* 161: 903–909.

Nicholson DM and Mathez EA (1991) Petrogenesis of the Merensky Reef in the Rustenburg section of the Bushveld Complex. *Contributions to Mineralogy and Petrology* 107: 293–309.

Nielsen RL (1992) BIGD.FOR – A fortran program to calculate trace-element partition coefficients for natural mafic and intermediate composition magmas. *Computers and Geosciences* 18: 773–788.

Nielsen TFD, Andersen JCO, and Brooks CK (2005) The Platinova reef of the Skaergaard intrusion. In: Mungall JE (ed.) *Exploration for Deposits of Platinum-Group Elements*, *Mineralogical Association of Canada Short Course Series*, vol. 35, pp. 431–455. Quebec: Mineralogical Association of Canada.

Nystrom JO and Henriquez F (1994) Magmatic features of iron-ores of the Kiruna type in Chile and Sweden – Ore textures and magnetite geochemistry. *Economic Geology* 89: 820–839.

O'Neill HSC and Mavrogenes JA (2002) The sulfide capacity and the sulfur content at sulfide saturation of silicate melts at 1400°C and 1 bar. *Journal of Petrology* 43: 1049–1087.

Peach CL and Mathez EA (1993) Sulfide melt silicate melt distribution coefficients for nickel and iron and implications for the distribution of other chalcophile elements. *Geochimica et Cosmochimica Acta* 57: 3013–3021.

Peach CL, Mathez EA, and Keays RR (1990) Sulfide melt silicate melt distribution coefficients for noble metals and other chalcophile elements as deduced from MORB – Implications for partial melting. *Geochimica et Cosmochimica Acta* 54: 3379–3389.

Philpotts AR (1967) Origin of certain iron-titanium oxide and apatite rocks. *Economic Geology* 62: 303–315.

Prendergast MD (2008) Archean komatiitic sill-hosted chromite deposits in the Zimbabwe Craton. *Economic Geology* 103: 981–1004.

Reid DL and Basson IJ (2002) Iron-rich ultramafic pegmatite replacement bodies within the Upper Critical Zone, Rustenburg Layered Suite, Northam Platinum Mine, South Africa. *Mineralogical Magazine* 66: 895–914.

Reynolds IM (1985) Contrasted mineralogy and textural relationships in the uppermost titaniferous magnetite layers of the Bushveld complex in the Bierkraal area north of Rustenburg. *Economic Geology* 80: 1027–1048.

Righter K, Campbell AJ, Humayun M, and Hervig RL (2004) Partitioning of Ru, Rh, Pd, Re, Ir and Au between Cr-bearing spinel, olivine, pyroxene and silicate melts. *Geochimica et Cosmochimica Acta* 68: 867–880.

Ripley EM, Brophy JG, and Li CS (2002) Copper solubility in a basaltic melt and sulfide liquid/silicate liquid partition coefficients of Cu and Fe. *Geochimica et Cosmochimica Acta* 66: 2791–2800.

Ripley EM, Severson MJ, and Hauck SA (1998) Evidence for sulfide and Fe-Ti-P-rich liquid immiscibility in the Duluth Complex, Minnesota. *Economic Geology* 93: 1052–1062.

Schoenberg R, Kruger FJ, Nägler TF, Meisel T, and Kramers JD (1999) PGE enrichment in chromitite layers and the Merensky Reef of the western Bushveld Complex: A Re–Os and Rb–Sr isotope study. *Earth and Planetary Science Letters* 172: 49–64.

Scoon RN and Eales HV (2002) Unusual Fe-Ti-Cr spinels from discordant bodies of iron-rich ultramafic pegmatite at the Amandelbult Platinum mine, northwestern Bushveld Complex. *Mineralogical Magazine* 66: 857–879.

Scoon RN and Mitchell AA (2004) Petrogenesis of discordant magnesian dunite pipes from the central sector of the eastern Bushveld Complex with emphasis on the Winnaarshoek pipe and disruption of the Merensky Reef. *Economic Geology* 99: 517–541.

Scoon RN and Teigler B (1994) Platinum-group element mineralization in the critical zone of the western Bushveld Complex. 1. Sulfide-poor chromitites below the UG-2. *Economic Geology* 89: 1094–1121.

Sillitoe RH and Burrows DR (2002) New field evidence bearing on the origin of the El Laco magnetite deposit, northern Chile. *Economic Geology* 97: 1101–1109.

Simon AC and Pettke T (2009) Platinum solubility and partitioning in a felsic melt–vapor–brine assemblage. *Geochimica et Cosmochimica Acta* 73: 438–454.

Smith MP and Henderson P (2000) Preliminary fluid inclusion constraints on fluid evolution in the Bayan Obo Fe-REE-Nb deposit, Inner Mongolia, China. *Economic Geology* 95: 1371–1388.

Sowerby JR and Keppler H (2002) The effect of fluorine, boron and excess sodium on the critical curve in the albite-H_2O system. *Contributions to Mineralogy and Petrology* 143: 32–37.

Spandler C, Mavrogenes J, and Arculus R (2005) Origin of chromitites in layered intrusions: Evidence from chromite-hosted melt inclusions from the Stillwater Complex. *Geology* 33: 893–896.

Spandler C, O'Neill H, St C, and Kamenetsky VS (2007) Survival times of anomalous melt inclusions from element diffusion in olivine and chromite. *Nature* 447: 303–306.

Tegner C, Cawthorn RG, and Kruger FJ (2006) Cyclicity in the Main and Upper Zones of the Bushveld Complex, South Africa: Crystallization from a zoned magma sheet. *Journal of Petrology* 47: 2257–2279.

Toplis MJ and Corgne A (2002) An experimental study of element partitioning between magnetite, clinopyroxene and iron-bearing silicate liquids with particular emphasis on vanadium. *Contributions to Mineralogy and Petrology* 144: 22–37.

Turner AR, Wolfgram D, and Barnes SJ (1985) Geology of the Stillwater county sector of the J-M reef, including the Minneapolis adit. In: Czamanske GK and Zientek ML (eds.) *The Stillwater Complex, Montana: Geology and Guide, Montana Bureau of Mines and Geology Special Publication* 92, pp. 210–230. Butte, MT: Montana Bureau of Mines and Geology.

Viljoen MJ and Hieber R (1986) The Rustenburg section of Rustenburg Platinum Mines Limited, with reference to the Merensky Reef. In: Anhaeusser CR and Maske S (eds.) *Mineral Deposits of Southern Africa*, vol. 2, pp. 1107–1134. Johannesburg: Geological Society of South Africa.

Weidner JR (1982) Iron-oxide magmas in the system Fe-C-O. *The Canadian Mineralogist* 20: 555–566.

Willmore CC, Boudreau AE, and Kruger FJ (2000) The halogen geochemistry of the Bushveld Complex, Republic of South Africa: Implications for chalcophile element distribution in the Lower and Critical zones. *Journal of Petrology* 41: 1517–1539.

Wykes JL and Mavrogenes JA (2005) Hydrous sulfide melting: Experimental evidence for the solubility of H_2O in sulfide melts. *Economic Geology* 100: 157–164.

Zhou M-F and Robinson PT (1997) Origin and tectonic environment of podiform chromite deposits. *Economic Geology* 92: 259–262.

Zhou M-F, Robinson PT, Lesher CM, Keays RR, Zhang C-J, and Malpas J (2005) Geochemistry, petrogenesis and metallogenesis of the Panzhihua gabbroic layered intrusion and associated Fe–Ti–V oxide deposits, Sichuan Province, SW China. *Journal of Petrology* 46: 2253–2280.

Zhou M-F, Robinson PT, Malpas J, and Li ZJ (1996) Podiform chromitites in the Luobusa ophiolite (southern Tibet): Implications for melt-rock interaction and chromite segregation in the upper mantle. *Journal of Petrology* 37: 3–21.

Zientek ML, Cooper RW, Corson SR, and Geraghty EP (2002) Platinum-group element mineralization in the Stillwater complex, Montana. In: Cabri LJ (ed.) *The Geology, Geochemistry, Mineralogy and Mineral Beneficiation of Platinum-Group Elements*, CIM Special Volume 54, pp. 459–481. Montreal: Canadian Institute of Mining, Metallurgy and Petroleum.